

172

# **VASIMR Engine Design for a Mission to Mars**

A project present to  
The Faculty of the Department of Aerospace Engineering  
San Jose State University

in partial fulfillment of the requirements for the degree  
*Master of Science in Aerospace Engineering*

By

**Mitesh D. Patel**

May 2011

approved by



Dr. Nikos Mourtos  
Faculty Advisor



**San José State**  
UNIVERSITY

Mitesh D. Patel

ALL RIGHTS RESERVED

The Designated Maters Project Committee Approves the Thesis Titled

VASIMR ENGINE DESIGN FOR A MISSION TO MARS

by

Mitesh D. Patel

APPROVED FOR THE MECHANICAL AND AEROSPACE ENGINEERING  
DEPARTMENT

SAN JOSÉ STATE UNIVERSITY

May 2011

---

Dr. Nikos Mourtos

Mechanical and Aerospace Engineering Department



Dr. Periklis Papadopoulos

Mechanical and Aerospace Engineering Department



Professor Nikola Djordjevic

Aero/Fluid/Performance Manager  
Lockheed Martin Space Systems Company

# ABSTRACT

## VASIMR ENGINE DESIGN FOR A MISSION TO MARS

by Mitesh D. Patel

Searching for life on another planet has been one of the mission objectives of the aerospace industry for a long time. Mars is the first outer planet and probably has water on the planet. This leads to the possibility of life on the planet. Previous missions gathered enough evidences to look for more details in future. There were few robotic missions to Mars in the past. The time has come for a manned mission to Mars but as conventional chemical rockets take months to reach the planet such mission has not been planned yet. The concept of VASIMR (Variable Specific Impulse Magneto-Plasma Rocket) would be very useful once developed to its full strength. It would take only forty days to reach Mars. It reduces the time for astronauts in the space hence it is less risky and practical to think of such manned missions. Moreover, the VASIMR would be less expensive than chemical rockets and would be able to carry heavier payloads. The aim of this project is to present the basic concepts of the VASIMR and design a rocket that is capable of going to Mars for future missions. VASIMR rocket has not been flown yet, however there is ongoing research and a VASIMR rocket is almost in the last stage of the complete development and it is expected to be launched in 2013. The trajectory design has been done using Star Travel software. Using the latest development and results from the AdastrA rocket company the further engine design has been done. Magnetic nozzle was designed by estimating the values of pressure and temperature values inside the engine. CAD drawings of the engine were made using Solid works.

## ACKNOWLEDGEMENT

I would like to take this opportunity to express my kind gratitude to all the people who have given their heart whelming full support in making this completion, a magnifying experience. Firstly, I thank God Almighty for granting me the patience and strength to get through this endeavor.

Secondly, I thank Dr. Nikos Mourtos, committee chairman and project advisor whose help, stimulating suggestions and encouragement helped me in all the time of research and writing of this report. He was abundantly helpful, offered invaluable assistance, support and guidance. He sincerely devoted his time and service for every activity and task that boosted my self esteem and taught me to be more responsible for my own good and as for others. I also thank the members of my graduate project committee for their guidance and suggestions. I would also like to thank San Jose State University and The department of Mechanical and Aerospace Engineering.

Lastly, I wish to express my love and gratitude to my parents for their unconditional & endless love and sense of understanding throughout the duration of my studies. They inspired and encouraged me at every step of my life by supporting me not just financially, but both morally and spiritually.

## Table of Contents

ABSTRACT.....	iv
ACKNOWLEDGEMENT.....	v
Nomenclature.....	viii
List of Figures.....	xi
List of Tables.....	xiii
1.0 Introduction.....	1
2.0 Literature Review.....	5
2.1 Life on Mars.....	5
2.2 Previous Missions to Mars.....	6
2.3 Possible Life on Mars.....	8
2.4 Previous and Proposed Work on VASIMR.....	9
2.5 Current research on the VASIMR engine.....	10
2.6 Detailed Study of VASIMR Engine.....	12
2.6.1 History and Future of VASIMR.....	12
2.6.2 VASIMR engine anatomy.....	14
2.6.3 Injection Stage (Helicon Discharge).....	15
2.6.4 The Heating Stage (ICRH-Ion Cyclotron Resonance Heating).....	15
2.6.5 The Nozzle.....	16
2.6.6 Magnetic Mirror.....	16
3.0 Trajectory Design.....	18

3.1 Interplanetary Transfer Orbit from Earth to Mars.....	18
3.2 Travel to the Mars.....	22
4.0 VASIMR engine.....	30
4.1 Selection of propellant.....	30
4.2 Injector.....	31
4.3 Helicon Stage.....	32
4.4 ICRH (Ion Cyclotron Resonance Heating).....	34
4.5 Magnetic Mirror.....	37
4.6 Magnetic Nozzle.....	37
4.6 Drawings.....	38
5.0 VASIMR Performance.....	44
5.1 Measurement of ionization Cost.....	44
5.2 Thruster Efficiency and Force.....	47
5.3 Efficiency Model.....	50
5.4 Coupling Efficiency.....	51
5.5 Nozzle and Magnetic Field.....	52
5.6 Mission Analysis.....	55
6.0 Conclusion and Recommendations.....	58
References:.....	59

## Nomenclature

$F$	Thrust [N]
$p_e$	Exit pressure [psi]
$p_o$	Outside pressure [psi]
$A_e$	Exit area [m <sup>2</sup> ]
$A_t$	Throat area [m <sup>2</sup> ]
$\dot{m}$	Mass flow rate [kg/s]
$\eta_n$	Nozzle efficiency [%]
$\eta_T$	Thruster efficiency [%]
$\eta_B$	Percent of second stage coupled RF power that becomes directed kinetic energy [%]
$\Gamma$	Total ion flux through the rocket [s <sup>-1</sup> ]
$\theta$	Half angle of the plume divergence [degrees]
$e$	Electron charge [1.60 * 10 <sup>-19</sup> C]
$E_1$	Kinetic energy of ions exiting first stage [eV]
$E_2$	Ion kinetic energy due to second stage heating [eV]
$E_i$	Ionization cost of the helicon stage [eV]
$F$	Total force measured in the plume [N]
$g$	Acceleration of gravity [9.81 m/s <sup>2</sup> ]
$I_{sp}$	Specific Impulse [s]
$m_{Ar}$	Mass of an argon atom [kg]
$P_1$	RF power coupled to the plasma in the first stage [W]
$P_2$	RF power coupled to the plasma in the second stage [W]

$P_{jet}$	Thruster jet power [W]
A	magnetic vector potential (Wb / m)
B	magnetic induction (0 – 5 Tesla)
C	speed of light ( $3 \times 10^8$ m / s)
E	electric field (Volt / m)
I	density tensor
i	imaginary unit
J	current (Ampere)
j	current density (0 – $10^5$ Ampere / m <sup>2</sup> )
$m_i$	particle mass ( $3.35 \times 10^{-27}$ kg for Deuterium ion)
n	plasma particle density (0 – $10^{20}$ m <sup>-3</sup> )
P	power (Watt)
p	power density (W / m <sup>2</sup> )
q	particle charge ( $1.6 \times 10^{-19}$ Coulomb)
R	resistance (0.2 Ohm – for circuit)
t	time (s)
ASPL	Advanced Space Propulsion Laboratory at NASA JSC
eV	electron-volt
ICRA	ion cyclotron resonant absorption
ICRF	ion cyclotron resonance frequencies
ICRH	ion cyclotron resonant heating
ICW	ion cyclotron wave
ISP	specific impulse
JSC	Johnson Space Center

LP	Langmuir probe
MPD	magnetoplasma dynamic
MSFC	Marshall Space Flight Center
ORNL	Oak Ridge National Laboratory
PRL	Propulsion Research Laboratory at NASA MSFC
RF	radio-frequency
RFC-LP	radio-frequency compensated Langmuir probe
RPA	retarding potential analyzer
VASIMR	Variable Specific Impulse Magnetoplasma Rocket
VX	VASIMR experiment

## List of Figures

Figure 1 Rocket thrust concept.....	2
-------------------------------------	---

Figure 2 Mars.....	3
Figure 3 Proposed VASIMR engine.....	9
Figure 4 Working of VASIMR engine.....	10
Figure 5 VASIMR Structure Concept.....	14
Figure 6 Magnetic Mirror.....	17
Figure 7 Hohmann transfer.....	19
Figure 8 Heliocentric transfer.....	20
Figure 9 Real time solar system calculator.....	21
Figure 10 Attempt with anomaly angles 0 & 110 degrees.....	24
Figure 11 Attempt with anomaly angles 45 & 150 degrees.....	25
Figure 12 Attempt with anomaly angles 39 & 81 degrees .....	26
Figure 13 Attempt with anomaly angles 60 & 91degrees.....	26
Figure 14 Difference in anomaly angles vs. Travel time.....	27
Figure 15 Moog type flow controller.....	30
Figure 16 Steady-state helicon discharge.....	31
Figure 17 Actual Helicon antenna.....	32
Figure 18 Profiles of density and temperature.....	32
Figure 19 Actual ICRH antenna.....	33
Figure 20 ICRF antenna improvement.....	34
Figure 21 ICRF performance dependence on the input ion flow rate.....	35
Figure 22 VASIMR Engine Solid works 3D drawing.....	38
Figure 23 VASIMR side view.....	39
Figure 24 VASIMR engine 3D view.....	39
Figure 25 Helicon antenna Drawing.....	40
Figure 26 Helicon antenna 3D view.....	40

Figure 27 ICRH antenna Drawing.....	41
Figure 28 ICRH 3D vie.....	41
Figure 29 Nozzle drawing.....	42
Figure 30 Nozzle 3D view.....	42
Figure 31 Ionization cost vs. RF Power.....	45
Figure 32 A color contour plot of the ionization cost of the helicon stage.....	46
Figure 33 Thruster Efficiency vs. Coupled RF Power and Thruster Efficiency vs. $I_{sp}$ .....	48
Figure 34 Force vs. $I_{sp}$ .....	49
Figure 35 2D contour plot of the plasma density $n(r,z)$ calculated by the particle trajectory code and magnetic configuration.....	52
Figure 36 2D contour plot of the plasma azimuthal velocity $V_{\phi}(r,z)$ cauculated by the particle trajectory code and magnetic configuration.....	53
Figure 37 2D contour plots of the diamagnetic current density $j_{p,\phi}$ , calculated by the particle trajectory code and the magnetic field lines for the corresponding diamagnetic plasma field $B_p$ .	53
Figure 38 2D plot of the magnetic induction configuration for the VASIMR.....	54

## List of Tables

Table 1 Historical Log of Mars Missions.....	6
--	---

Table 2 VASIMR development stage.....	13
Table 3 Calculated parameters.....	28
Table 4 Propellant properties and parameters.....	29
Table 5 ICRH performance for different configuration.....	35
Table 6 Ionization cost relative to Power.....	44
Table 7 $I_{sp}$ -Force table.....	48

## 1.0 Introduction

The Aerospace industry took a long time to grow since it started in the first decade of nineteenth century. Few inventions occurred at regular time interval that demonstrated such technology, which made the following milestones available: Hypersonic flight, Supersonic transport jets, Landing on other planets, and orbiting around Earth. The history of an aerospace industry has been included in this chapter. It also introduces the topic of the project and mentions the motivation for choosing it. Moreover, it informs about the plan, timeframe, scope, people who helped, and the place while working on project.

One of the biggest achievements of human beings has been to reach the moon. Aircrafts and spacecrafts have made a whole new world of research available. More than just as a career option it is an area of interest and passion. The Wright brothers created history on December 17, 1903 by flying the first airplane. After one hundred and seven years since the first flight, aerospace industry has grown more than anything else. Man stepping on the moon in 1969 has been one of the biggest milestones in the history of rockets and spacecrafts.

Searching for life on another planet has been a mission objective for a long time for many of the rocket missions. There were missions which only completed on the paper. The cost and less possibility for success made denial of implementing those projects. Searching for life on another planet is not just an interesting topic for the aerospace industry, perhaps biology, and chemistry has more interest in learning about these planets and life. Aliens from another planet have been seen on Earth made us curious for searching a planet that has life on it. Possibility of life on the Mars and moon of Jupiter is expected because of the conditions on them. To search for life on Mars scientific instruments must reach and collect information on the surface of Mars.

A rocket that can carry all instruments and perhaps men safely to Mars is the first need for mission. The project topic has been selected to design such a rocket that can go to the Mars.

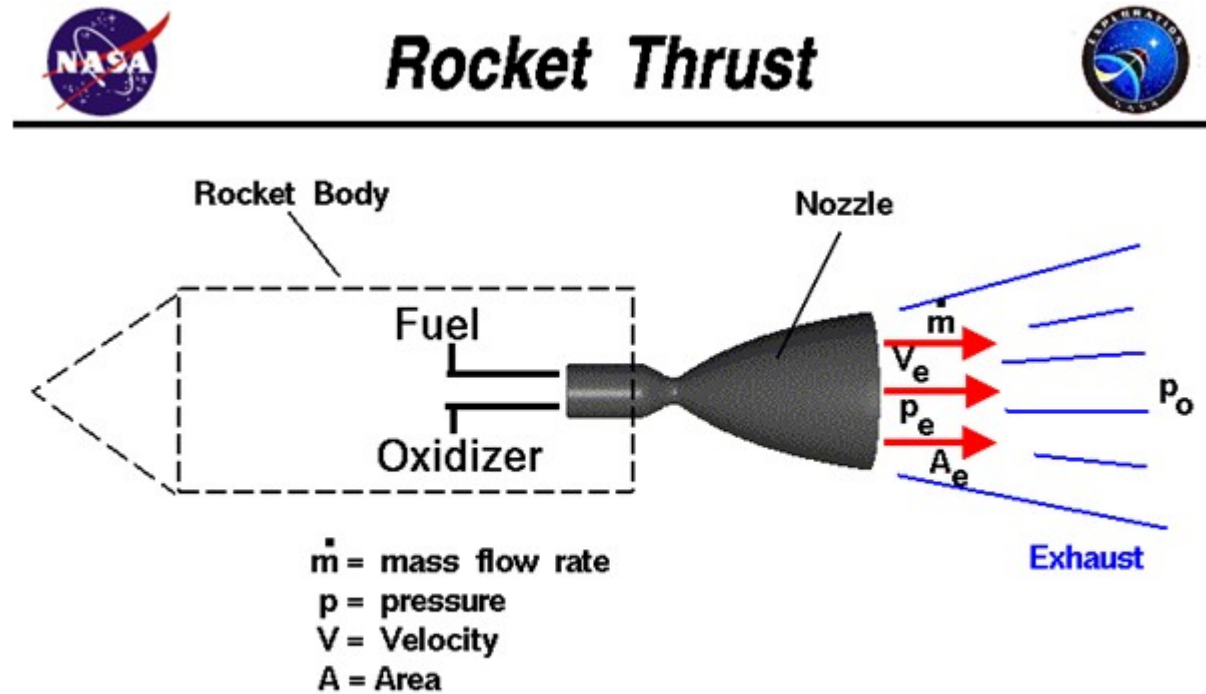


Figure 1 Rocket thrust concept Source: NASA, 2010

$$Thrust = T = \dot{m} V_e + (p_e - p_o) A_e \quad (1)$$

A rocket engine or simply "rocket" is a jet engine that uses only propellant mass for forming its high speed propulsive jet. Rocket engines are reaction engines and obtain thrust in accordance with Newton's third law. A rocket engine design is the most important aspect of any project that is designed to go in the space. Rockets generate such power that takes the spacecraft or satellite out of the atmosphere. Equation (1.1) is the thrust equation. Figure 1 explains the basic geometry of rocket and how thrust is generated. Rocket engine design is a vast area to

concentrate. Principal of operation, overall rocket engine performance, cooling, mechanical issues, acoustic issues, safety, testing, ignition are some of the very important aspects of rocket engine design.

A mission to carry man to the Mars and to perform science there and bring them back to the Earth is one of the biggest challenges an aerospace industry has ever had. Most of the developed countries are working on the project to discover life on Mars. In order to complete actual mission with all available instruments, and systems, they all must reach safely on the surface of Mars. A rocket must be designed to take these systems and man to Mars.

Mars is the fourth planet from the Sun in Solar system. It is the first outer planet. The planet is named after the Roman god of war, Mars. It is often described as the "Red Planet", as the iron oxide prevalent on its surface gives it a reddish appearance. Mars is a terrestrial planet with a thin atmosphere, having surface features reminiscent both of the impact craters of



the Moon and the volcanoes, valleys, deserts, and polar ice caps of Earth. The rotational period and seasonal cycles of Mars are likewise similar to those of Earth.

For hundreds of years our observations of Mars were restricted by the vast distance separating Earth from the red planet. About once every two years, at its closest approach

(called opposition), Mars passes within about 55 million km of Earth and it is then that we are

able to

capture pictures of maximum resolution with earth-based telescopes.

The Hubble Space Telescope now provides us with excellent views from earth-orbit, but until the launching of probes to Mars to collect and relay data back to Earth, much of what was "known" about Mars was based on fuzzy pictures which showed only large scale planetary features and events. Some of the earth-based observations were: orbital and rotational dynamics, atmospheric phenomena, seasonal variations in the polar caps, variations in surface color (which were

Figure 2 Mars Source: Google, 2010

explained by theories ranging from the presence of vegetation, to water bodies linked by martian-made canals, to variations in surface composition); all of which resulted in a variety of interpretations. Atmospheric pressure and composition, as well as surface temperature, was studied using spectroscopy, but there was much debate about the varied results obtained by different studies.

The earth-based observations of Mars paved the way for spacecraft exploration of the planet. So many questions had been raised about Mars and there were so few answers. Did life exist on Mars in the past or present? Was water present on the planet? If so, what form was it in? What was the atmosphere composed of and what were its dynamics? Could Mars be used to tell us more about the evolution of both Earth and our solar system? These were some of the questions which captured the imaginations of scientists from many disciplines, and the answers could only be found by direct observation. Judging by the reaction to the H.G. Wells "War of the Worlds" radio broadcast, the public was not immune to the mysteries of Mars either. Fueled by the curiosities of both the scientific community and the public, on November 28, 1964 at 9:22 EST Mariner 4 was launched and 228 days later it would become the first spacecraft ever to visit

the red planet. Numbers of mission to Mars have been attempted in the past and some of them were successful.

## **2.0 Literature Review**

This chapter includes detailed information on life on other planet, conditions on Mars, previous and proposed work on rockets, and current research on similar projects. The current research includes how the other people working on same project. Their approach, methods, expectations, and problems are strong references for getting started. This chapter successively narrows the topics and ends to the project title.

### **2.1 Life on Mars**

There was an old belief that: “The only planet that has life is Earth.” It is not true exist anymore. Aliens have been seen on Earth at different times forced us not to believe in that belief. The full form of UFO is Unidentified Flying Object. The flying objects that are difficult to identify are known as UFO. UFOs seen on the Earth proves the existence of aliens. These aliens are from another planet. Moreover, discovery of the Mars atmospheric conditions in 2001 opened the scope of discovering life on mars. The NASA Mars Odyssey program successfully gathered important information of the planet.

2001 Mars Odyssey has contributed numerous science results. It has mapped the amount and distribution of chemical elements and minerals that make up the martian surface. Maps of hydrogen distribution led scientists to discover vast amounts of water ice in the Polar Regions buried just beneath the surface. Odyssey has also recorded the radiation environment in low Mars orbit to determine the radiation-related risk to any future human explorers who may one day go to Mars (NASA/JPL, March 2010).

A robotic lander which landed on the surface of mars was unable to discover life. Still there are projects under progress for discovering life on mars.

## 2.2 Previous Missions to Mars

There were missions to mars with different mission objectives at different times. They were as shown in the table below.

Table 1 Historical Log of Mars Missions

Launch Date	Name	Country	Result	Reason
1960	Korabl 4	USSR (flyby)	Failure	Didn't reach Earth orbit
1960	Korabl 5	USSR (flyby)	Failure	Didn't reach Earth orbit
1962	Korabl 11	USSR (flyby)	Failure	Earth orbit only; spacecraft broke apart
1962	Mars 1	USSR (flyby)	Failure	Radio Failed
1962	Korabl 13	USSR (flyby)	Failure	Earth orbit only; spacecraft broke apart
1964	Mariner 3	US (flyby)	Failure	Shroud failed to jettison
1964	Mariner 4	US (flyby)	Success	Returned 21 images

1964	Zond 2	USSR (flyby)	Failure	Radio failed
1969	Mars 1969A	USSR	Failure	Launch vehicle failure
1969	Mars 1969B	USSR	Failure	Launch vehicle failure
1969	Mariner 6	US (flyby)	Success	Returned 75 images
1969	Mariner 7	US (flyby)	Success	Returned 126 images
1971	Mariner 8	US	Failure	Launch failure
1971	Kosmos 419	USSR	Failure	Achieved Earth orbit only
1971	Mars 2 Orbiter/Lander	USSR	Failure	Orbiter arrived, but no useful data and Lander destroyed
1971	Mars 3 Orbiter/Lander	USSR	Success	Orbiter obtained approximately 8 months of data and lander landed safely, but only 20 seconds of data
1971	Mariner 9	US	Success	Returned 7,329 images
1973	Mars 4	USSR	Failure	Flew past Mars
1973	Mars 5	USSR	Success	Returned 60 images; only lasted 9 days
1973	Mars 6 Orbiter/Lander	USSR	Success/Failure	Occultation experiment produced data and Lander failure on descent
1973	Mars 7 Lander	USSR	Failure	Missed planet; now in solar orbit.

1975	Viking 1 Orbiter/Lander	US	Success	Located landing site for Lander and first successful landing on Mars
1975	Viking 2 Orbiter/Lander	US	Success	Returned 16,000 images and extensive atmospheric data and soil experiments
1988	Phobos 1 Orbiter	USSR	Failure	Lost en route to Mars
1988	Phobos 2 Orbiter/Lander	USSR	Failure	Lost near Phobos
1992	Mars Observer	US	Failure	Lost prior to Mars arrival
1996	Mars Global Surveyor	US	Success	More images than all Mars Missions
1996	Mars 96	USSR	Failure	Launch vehicle failure
1996	Mars Pathfinder	US	Success	Technology experiment lasting 5 times longer than warranty
1998	Nozomi	Japan	Failure	No orbit insertion; fuel problems
1998	Mars Climate Orbiter	US	Failure	Lost on arrival
1999	Mars Polar Lander	US	Failure	Lost on arrival
1999	Deep Space 2 Probes (2)	US	Failure	Lost on arrival (carried on Mars Polar Lander)
2001	Mars Odyssey	US	Success	High resolution images of Mars
2003	Mars Express Orbiter/Beagle 2 Lander	ESA	Success/Failure	Orbiter imaging Mars in detail and lander lost on arrival

2003	Mars Exploration Rover - Spirit	US	Success	Operating lifetime of more than 15 times original warranty
2003	Mars Exploration Rover - Opportunity	US	Success	Operating lifetime of more than 15 times original warranty
2005	Mars Reconnaissance Orbiter	US	Success	Returned more than 26 terabits of data (more than all other Mars missions combined)
2007	Phoenix Mars Lander	US	Success	Returned more than 25 gigabits of data

Only few of them were successful. First successful mission was Mariner 4 in 1964. It successfully captured 21 images and the last successful mission was Phoenix in 2007 which took 25 gigabits of pictures.

### 2.3 Possible Life on Mars

Earth's history is recorded in its rocks. Layers of sediment, compressed and cemented to form rock, tell tales of the comings and goings of seas, mountain ranges, rivers, volcanoes, and deserts. Earth's sedimentary rocks record changes in climate and biodiversity over time. Most of what is known about Earth's past comes from the study of layered rock and the materials--- grains, structures, and fossils---found within them.

Mars Global Surveyor (MGS), Mars Orbiter Camera (MOC) images have very high resolution, allowing detection of objects the size of school buses and airplanes. Such images are comparable to the aerial photographs used by geologists on Earth to plan their fieldwork in areas of layered sedimentary and volcanic rock. Hundreds of MOC images have revealed outcrops of layered rock exposed by erosion and faulting in craters and chasms on the red planet.

Martian sedimentary rocks are just now beginning to reveal clues about the planet's complex early history. "Early Mars" refers to a time thought to have been more than 3.5 billion years ago, a period when the planet was young and impact craters---created by meteors, asteroids, and comets hitting the surface---were forming more frequently than they do today.

The history suggested by the martian sedimentary rocks may have included warm, wet climates with thousands of crater lakes (*i.e.*, with liquid water) that persisted for millions of years. Alternatively, the rocks might be recording climate changes and thick deposits of airborne dust formed on a much colder, drier world than many have suspected. In either case, the images indicate that early Mars was very different from the planet today, and its history---recorded in rocks---beckons further exploration.

## **2.4 Previous and Proposed Work on VASIMR**

For space mission solid and liquid rockets are widely used. These two types are less expensive compared to other types, but they are not good enough for mission to carry huge structures, and weight for very long distance. Moreover, they are not efficient as Variable Specific Impulse Magnetoplasma Rocket (VASIMR), and Nuclear thermal rocket. These two are new concepts of rocket engine. A combination of liquid, solid rocket is still good enough just to take the payload to outer space. The concentration on designing an engine that can take payload

from the space to surface of Mars is the prime objective of this project.

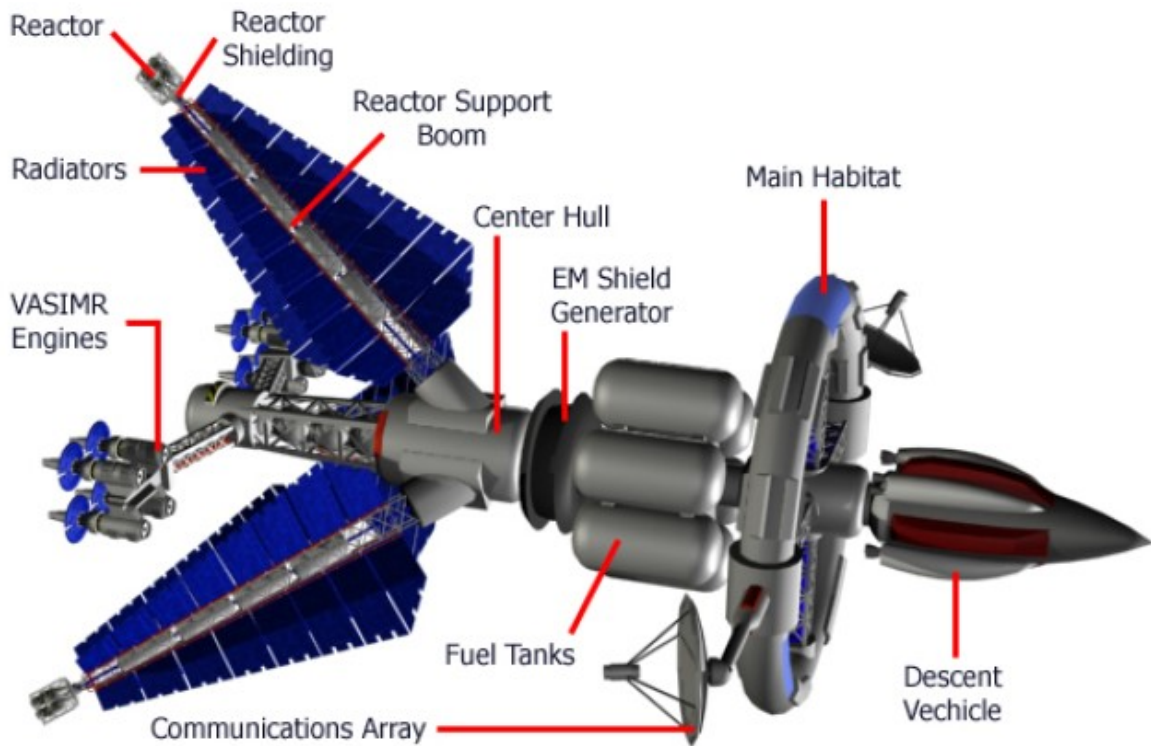
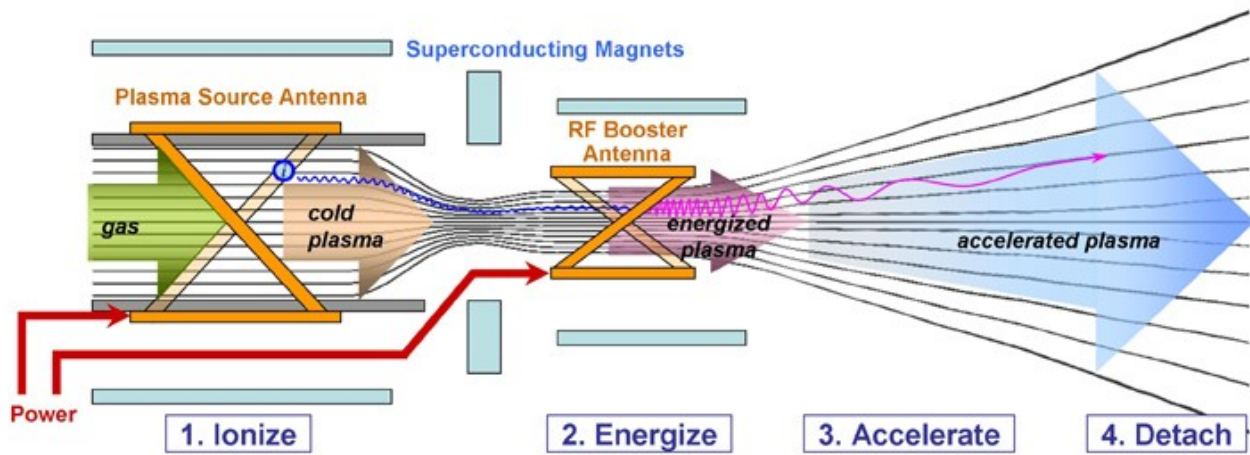


Figure 3 Proposed VASIMR engine Source: Atkov, 2004

For a mission to Mars, a VASIMR is suggested because of its highly efficient characteristic. Figure 3 shows the proposed design of the rocket with the entire payload inserted



on it. It has a descent vehicle that carries a lander. Moreover, the rocket carries an orbiter to transmit the data back to Earth. The figure clearly shows the location of each part.

Figure 4 explains the concept of VASIMR engine. Figure includes four successive  
 Figure 4 Working of VASIMR engine Source: Adastr, August 31, 2010

processes ionize, energize, accelerate, and detach. In the ionize phase the cold gas enters the process, whereas after detach accelerated plasma comes out of the nozzle which leads to high thrust. Rocket engine design comes under propulsion. Propulsion also includes any kind of engine design that has to deal in propelling the vehicle.

## 2.5 Current research on the VASIMR engine

After many years researching the concept with NASA, Franklin Chang-Diaz set up the Ad Astra Rocket Company in January 2005 to begin development of the VASIMR engine. Later that year, the company signed a Space Act Agreement with NASA, and were granted control of the

Advanced Space Propulsion Laboratory. In this lab, a 50 kW prototype was constructed, and underwent testing in a vacuum chamber. Later, a 100 kW version was developed, and this was followed by a 200 kW prototype. After a long period of rigorous testing in a 150 m<sup>3</sup> vacuum chamber, the latest configuration was deemed space-worthy, and it was announced that the company had entered into an agreement to test the engine on the International Space Station, in or before 2013.(Cipolla, 2008)

The first VASIMR engine model VX-50 proved to be capable of 0.5 newtons (0.1 lbf) thrust According to company's data, current VASIMR efficiency was then at 67%. Published data on the VX-50 engine, capable of processing 50 kW of total radio frequency power, showed efficiency to be 59% calculated as: 90%  $N_A$  ion generation efficiency  $\times$  65%  $N_B$  ion speed boosting efficiency. It was hoped that the overall efficiency of the engine could be increased by scaling up power levels.

A recent press release on November 23, 2010 released the latest information on the development of VX-200. It has successfully achieved the thrust force of 5.7N, 50 km/s exhaust speed, at VASIMR efficiency of 72%. This article shows the current results in 200 kW engine which leads to the first mission to international space station in 2013.(AdAstra, Nov, 2010)

The 2013 VASIMR test on the International Space Station is expected to lead to multiple and immediate revenue producing applications: (VASIMR, Aug 28, 2010)

1) Capability of maintaining the International Space Station in a stable orbit at 1/20th of the approximately \$210 million/year present estimated cost.

2) Improvements in a variety of satellite mission applications, including plane changes, increased maneuverability and speed of completion, refueling, repair, ultimate disposal over present capabilities.

3) In a combined chemical- VASIMR transfer stage, it could nearly triple the payload delivery to the Moon as compared to an all chemical approach.

4) In a solar-boosted mission design concept, proposed by Ad Astra, VASIMR decreases the transit time of a mission to the Jupiter system to 1/5 of the all chemical mission approach (including a gravity assist)

## **2.6 Detailed Study of VASIMR Engine**

### **2.6.1 History and Future of VASIMR**

Scientist and former astronaut Franklin Chang-Diaz created the VASIMR concept and has been working on its development since 1977. The idea came in his mind when he was involved in the study of magnetic ducts and their application to controlled nuclear fusion. VASIMR rocket is under research and development since then. It has now in a stage that, the Ad Astra Company will be testing an actual rocket to the international space station in 2013. After years of research at NASA, Franklin Chang-Diaz set up the Ad Astra Rocket Company in January 2005 to begin development of the VASIMR engine. The Company was granted control of the Advanced Space Propulsion Laboratory. It started with 50kW prototype, they constructed 100kW version. Most recently last year they successfully made a test run for 200kW engine. Major milestones in this test program have been achieved as listed: (Andrew, 2010)

Table 2 VASIMR development stage

Development Stage	Time
First Plasma	May 2008
Full(30kW) first stage power demo	Oct 2008
Second stage integration	Jan 2009
VX-200 full (2 Tesla) Magnetic field	July 2009
VX-200 at full (200kW) rated power	Oct 2009

VASIMR is not suitable to launch payloads from the surface of the Earth due to its low thrust to weight ratio and its need of a vacuum to operate. Instead, it would function as an upper stage for cargo, reducing the fuel requirements for in-space transportation. The engine is expected to perform the following functions at a fraction of the cost of chemical technologies: (Executive Summary, 2008).

- Drag compensation for space stations
- Lunar cargo delivery
- Satellite repositioning
- Satellite refueling, maintenance and repair
- In space resource recovery
- Ultra fast deep space robotic missions

The VASIMR engine is expected to bring a revolutionary change in going to other planets and deep space. Mission to Mars, Moon and Europa will be possible in relatively low mission time compared to chemical or other rockets.

## 2.6.2 VASIMR engine anatomy

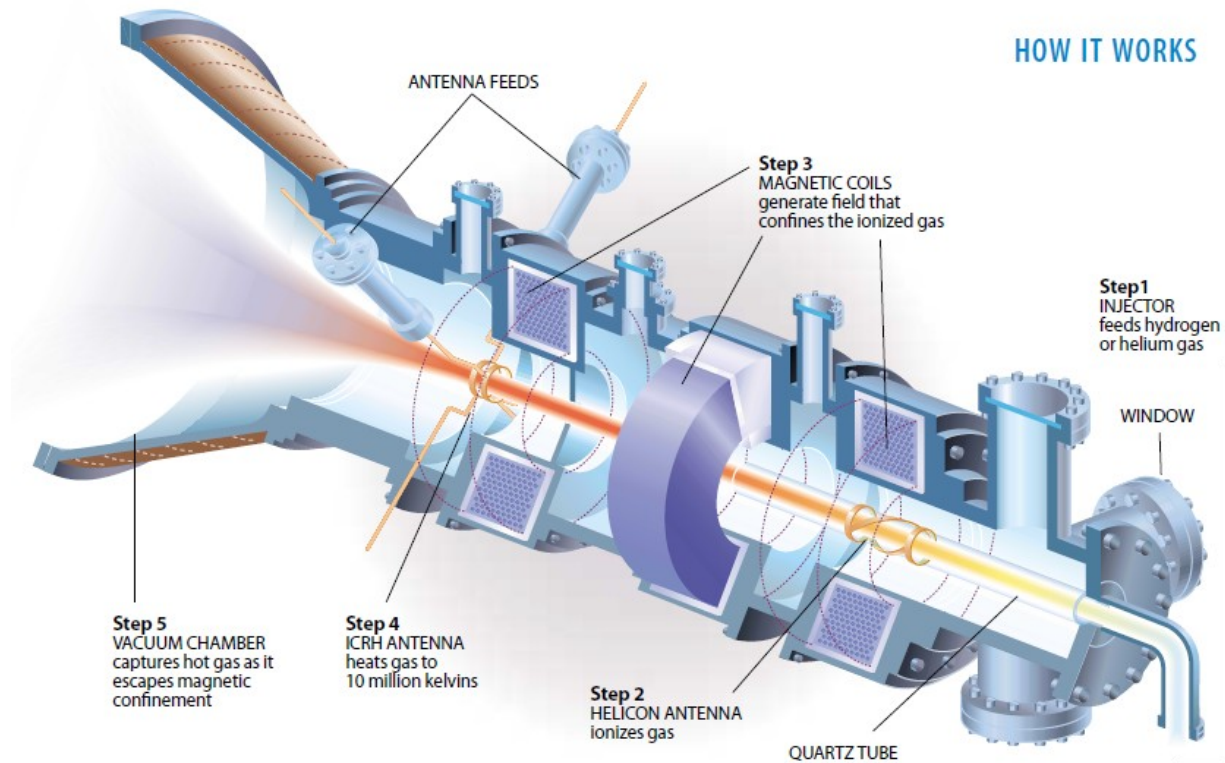


Figure 5 VASIMR Structure Concept Source: The VASIMR rocket, 2000

The VASIMR engine consists of three main sections: A helicon Plasma source, an ICRH plasma accelerator, and a magnetic nozzle. The VASIMR does not use electrodes in design, which makes it suitable for high power density and long component life by reducing plasma erosion and other material complications.

The magnetic field ties the three stages together and, through the magnet assemblies, transmits the exhaust reaction forces that propel the ship. The plasma is produced by an integrated helicon discharge. The bulk of plasma energy is added in a separate downstream stage by ion cyclotron resonance heating (ICRH). Axial momentum is obtained by the adiabatic expansion of the plasma in a magnetic nozzle. Thrust/specific impulse ratio control in the

VASIMR is primarily achieved by the selective partitioning of the RF power to the helicon and ICRH systems, with the proper adjustment of the propellant flow.(VASIMR, 2009, 011009)

The three major subsystems in a VASIMR engine are: injection stage, the heating stage, and the nozzle.

### **2.6.3 Injection Stage (Helicon Discharge)**

A helicon is a low frequency electromagnetic wave. A helicon discharge can be defined as an excitation of plasma by helicon waves induced through radio frequency heating. The presence of this magnetic field creates a helicon mode of operation with higher ionization efficiency and greater electron density. Most plasma rockets require physical electrodes, which erode quickly in the harsh environment. In contrast, VASIMR uses radio antennas. The radio waves heat the plasma just like a microwave oven heats food. Two wave processes come into play. First, neutral gas in the injector stage becomes dense and comparatively cold (about 60,000 Kelvin) (VASIMR, 2009, 241008) plasma through the action of helicon waves. These are electromagnetic oscillations at frequencies of 10 to 50 MHz, which, in a magnetic field, energize free electrons in a gas. The electrons quickly multiply by liberating other electrons from nearby atoms in a cascade of ionization.

### **2.6.4 The Heating Stage (ICRH-Ion Cyclotron Resonance Heating)**

The next stage downstream is the heating system. Energy is fed to the system in the form of a circularly polarized RF signal tuned to the ion cyclotron frequency. ICRH heating has been chosen because it transfers energy directly and primarily to the ions, which maximizes the efficiency of the engine. Ion cyclotron resonance is a phenomenon related to the movement of ions in a magnetic field. Cyclotron frequency is the frequency of a charged particle moving perpendicularly to the direction of a uniform magnetic field, i.e. a magnetic field of constant magnitude and direction. Since that motion is always circular, the cyclotron frequency is well defined. An electron in a static and uniform magnetic field will move in a circle due to the Lorentz force. The circular motion may be superimposed with a uniform axial motion, resulting in a helix, or with a uniform motion perpendicular to the field. An important consideration involves the rapid absorption of ion cyclotron waves by the high-speed plasma flow. (Glover, 2010)

### **2.6.5 The Nozzle**

While the cyclotron heating process results in approximately thermalized ion energy distributions, the non-linear absorption of energy in the single-pass process produces a boost, or displacement of the ion kinetic energy distribution. The ions are immediately ejected through the magnetic nozzle before the ion distribution has had time to thermalize. Similar to the physical nozzles of chemical propulsion systems, magnetic nozzles are the critical acceleration stage of numerous plasma propulsion systems currently in development. A diverging magnetic field is used to convert plasma's thermal energy into directed kinetic energy, while also confining the

energetic plasma away from the surfaces of the thruster. Magnetic nozzles are a desirable acceleration mechanism because they do not require the use of electrodes, which are often the lifetime limiting component of plasma propulsion systems.

### 2.6.6 Magnetic Mirror

VASIMR embodies a class of magnetic ducts called magnetic mirrors. The simplest magnetic mirror is produced by two ring electromagnets with current flowing in the same direction. The magnetic field is constricted near the rings but bulges out in between them.

Charged particles move in a helix along field lines, orbiting around them at a specific radius, the Larmor radius, and at the so-called cyclotron frequency. As one might expect, for a field of a given strength, the heavier particles (the ions) have a lower cyclotron frequency and larger

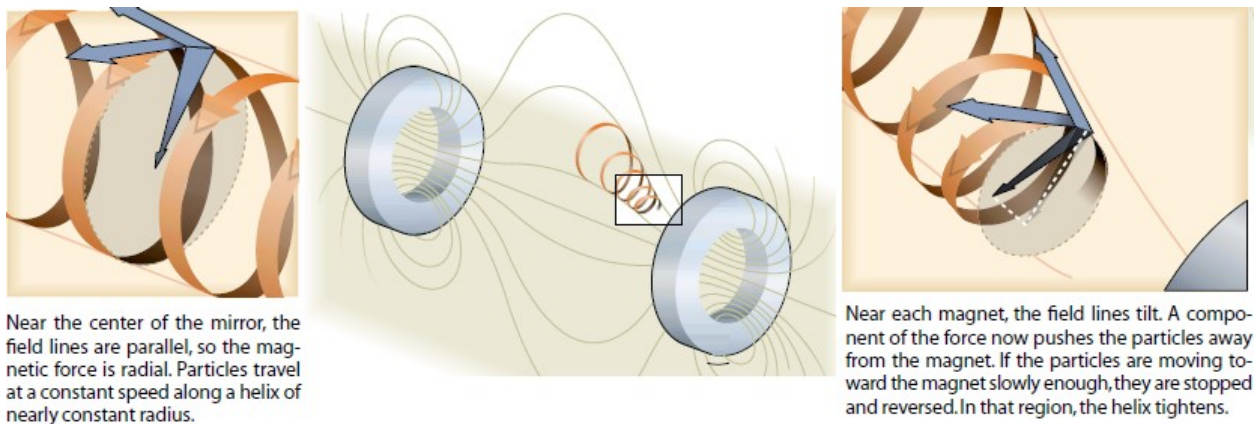


Figure 6 Magnetic Mirror Source: The VASIMR rocket, 2000

larmor radius than the light ones (the electrons) do. Also, strong fields lead to a high cyclotron frequency and small Larmor radius. In VASIMR, the ion cyclotron frequency is a few megahertz (MHz), whereas its electron equivalent is in the gigahertz range. The particles' velocity has two components: one parallel to field (corresponding to the forward motion along the field line) and the other perpendicular (corresponding to the orbital motion around the line). When a particle approaches a constricted (hence stronger) field, its perpendicular velocity increases, but its parallel one is reduced proportionately to keep the total energy constant. The reason has to do with the direction of the force exerted by the field on the particle. The force is always perpendicular to both the particle's velocity and the field direction. Near the center of the mirror, where the field lines are parallel, the force is radial and so has no effect on the parallel velocity. But as the particle enters the constriction, the force tilts away from the constriction, resulting in an imbalance that decelerates the particle. If the particle is exiting the constriction, the field has the opposite effect and the particle accelerates. Because no energy has been added, the acceleration comes at the expense of rotational motion. The magnetic field does not work on the particle; it is simply a vehicle enabling this energy transfer. (Chang, 2010)

### **3.0 Trajectory Design**

A trajectory is the path a moving object follows through space as a function of time. The object might be a projectile or a satellite, for example. It thus includes the meaning of orbit—the path of a planet, an asteroid or a comet as it travels around a central mass. A trajectory can be

described mathematically either by the geometry of the path, or as the position of the object over time.

### **3.1 Interplanetary Transfer Orbit from Earth to Mars**

Transfer orbits from Earth to most of the planets in the solar system may be considered to be elliptical and co-planar. Two types of orbit transfer are:

(1) Hohmann Transfer

(2) Heliocentric Transfer

A Hohmann Transfer between Earth and Mars may be achieved when the elliptical transfer orbit is tangent to Earth's orbit at departure ( $V_1=0$  deg) and tangent to Mars orbit at arrival ( $V_2=180$  deg). This kind of interplanetary transfer orbit is called a Hohmann Transfer and represents the minimum delta-velocity ( $dV$ ) required for Mars orbital insertion from Earth orbit. A hohmann transfer orbit is as shown in figure 7 below. The figure shows a snapshot of a hohmann transfer from Earth to Mars. It shows the time taken to reach Mars is 259 days.

**StarTravel 3.0: Orbital Mechanics and Relativistic Star Travel by AeroRocket**

File Units Trajectory-Selections Planetary-plots

### Interplanetary Transfer Orbit From Earth

Destination planet for heliocentric transfer: **MARS**

True anomaly at origin planet ( $\nu_1$ )	0.0	DEGREES
True anomaly at destination planet ( $\nu_2$ )	180.0	DEGREES
Burnout altitude at origin planet (Hb)	300.0	KM
Destination planet miss distance (X)	0.0	KM
Spacecraft burnout velocity ( $V_b$ )	11561.49	M/SEC
Radius from Sun to Earth (R1)	1.496E+11	M
Radius from Sun to planet (R2)	2.2799E+11	M
Escape velocity from Earth surface ( $V_e$ )	11179.88	M/SEC
Earth orbital velocity around Sun ( $V_{cs}$ )	29783.12	M/SEC
Orbital velocity around Sun at burnout ( $V_1$ )	32729.02	M/SEC
dV for transfer orbit insertion: $dV = V_1 - V_{cs}$	2945.9	M/SEC
Velocity of approach on transfer ellipse ( $V_2$ )	21475.73	M/SEC
Flight path angle between $V_{cs}$ and $V_1$	0.	DEGREES
Time of flight from burnout to intercept (T)	258.93	DAYS

**Solar System Calculator**

Maximum time from present, Earth years:

Elapsed time from present, Earth years:

**11/30/2010 8:16:29 PM**

	Distance (M)	T (yrs)
Mars		
Jupiter		
Saturn		
Uranus		
Neptune		
Pluto		

**ZOOM**

	Distance (M)	T (yrs)
Mercury		
Venus		
Earth		

**EARTH - MARS**

Interplanetary Transfer Orbits: Transfer orbits to most of the planets may be considered to be circular and coplanar. A Hohmann transfer between Earth and Mars as defined when the transfer orbit is tangent to Earth's orbit at departure and tangent to Mars orbit at arrival represents the minimum delta-v required for Mars insertion. Other heliocentric orbits to the planets are possible if orbits intersect.

Hohmann transfer analysis complete.

## Figure 7 Hohmann transfer

Heliocentric (around the Sun) orbits to Mars and the other planets are possible if the transfer orbit intersects both the origin planet orbit and the destination planet orbit. Figure-8 displays the general concept of a heliocentric transfer orbit when the true anomaly of the origin planet ( $V_1$ ) is non-zero and the true anomaly of the destination planet ( $V_2$ ) is something other than 180 degrees. During a heliocentric or Hohmann transfer an interplanetary spacecraft spends most of its flight time under the gravitational influence of a single body - the Sun. Only during orbital insertion the destination planet's gravitational field becomes significant.

**StarTravel 3.0: Orbital Mechanics and Relativistic Star Travel by AeroRocket**

File Units Trajectory-Selections Planetary-plots

### Interplanetary Transfer Orbit From Earth

Destination planet for heliocentric transfer: **MARS**

True anomaly at origin planet ( $\nu_1$ )	39	DEGREES
True anomaly at destination planet ( $\nu_2$ )	81	DEGREES
Burnout altitude at origin planet (Hb)	300.0	KM
Destination planet miss distance (X)	0.0	KM
Spacecraft burnout velocity (Vb)	20199.35	M/SEC
Radius from Sun to Earth (R1)	1.496E+11	M
Radius from Sun to planet (R2)	2.2799E+11	M
Escape velocity from Earth surface (Ve)	11179.88	M/SEC
Earth orbital velocity around Sun (Vcs)	29783.12	M/SEC
Orbital velocity around Sun at burnout (V1)	41794.78	M/SEC
dV for transfer orbit insertion: $dV = V1 - Vcs$	16823.32	M/SEC
Velocity of approach on transfer ellipse (V2)	33716.79	M/SEC
Flight path angle between Vcs and V1	19.219	DEGREES
Time of flight from burnout to intercept (T)	47.627	DAYS

Solar System

Maximum time from present, Earth years: 0

Elapsed time from present, Earth years: .0

11/30/2010 9:22:23 PM

Distance (M) T (yrs)

Mars		
Jupiter		
Saturn		
Uranus		
Neptune		
Pluto		

Mercury --- Distance (M) T (yrs)

Mercury		
Venus		
Earth		

**EARTH - MARS**

Interplanetary Transfer Orbits: Transfer orbits to most of the planets may be considered to be circular and coplanar. A Hohmann transfer between Earth and Mars as defined when the transfer orbit is tangent to Earth's orbit at departure and tangent to Mars orbit at arrival represents the minimum delta-v required for Mars insertion. Other heliocentric orbits to the planets are possible if orbits intersect.

Hohmann transfer analysis complete.

## Figure 8 Heliocentric transfer

The patched-conic method is sometimes used to compute destination planet orbital insertion when the spacecraft is within the sphere of influence of the destination planet. The simplification is achieved by dividing space into various parts by assigning each of the  $n$  bodies (e.g. the Sun, planets, moons) its own sphere of influence. When the spacecraft is within the sphere of influence of a smaller body, only the gravitational force between the spacecraft and that smaller body is considered, otherwise the gravitational force between the spacecraft and the larger body is used. This reduces an unsolvable  $n$ -body problem to multiple solvable two-body problems, for which the solutions are the well-known conic sections of the Kepler orbits. However, the patched-conic method is not used to determine destination planet orbital insertion. Finally, perturbations caused by the other planets in the solar system while the spacecraft is in its heliocentric course are negligible. Under these assumptions, the two-body orbital analysis used by Star Travel is a valid assumption for general time of flight (T) and  $dV$  requirements for orbital transfers and fly-bys between planets.

Star Travel gives an option to see the relative position of all the planets and sun after certain amount of time. This option allows us to animate the solar system which shows the relative rotation of planets around the earth. In there are two operating parameters in which one shows the maximum amount of time that we can enter to see the animation for that specific amount of time in years whereas the other box shows elapsed no of years. The time is in earth years.

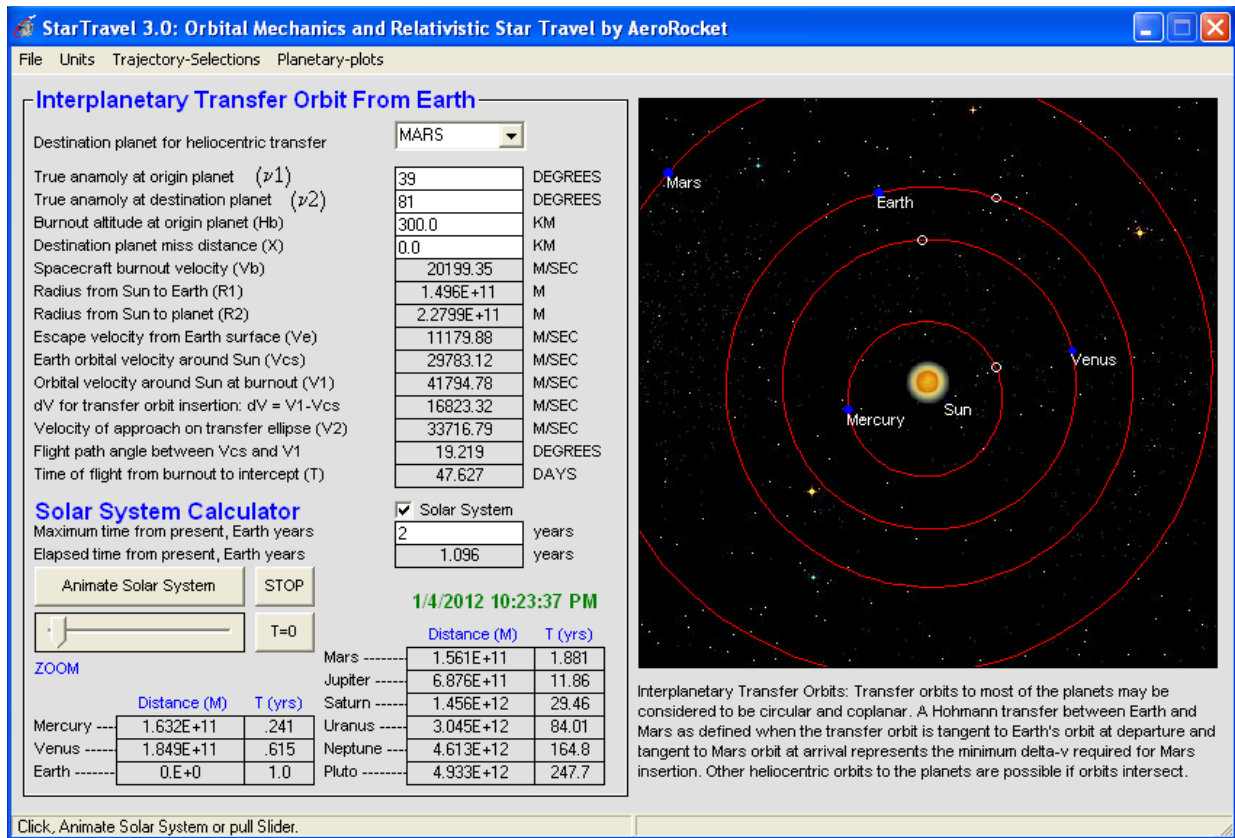


Figure 9 Real time solar system calculator

This option allows seeing the relative position of planets after certain amount of time. Figure 9 gives an idea about its usefulness. In this figure the solar system was given 2 years of time for the animation. And the stop button allows us to stop the animation at any given time during the animation. In this manner we can see the closest approach of planets relative to each other and can tell about the closest approach in future.

### 3.2 Travel to the Mars

To reach an outer planet (i.e. Mars), a spacecraft must be launched from Earth at a velocity greater than the planetary escape velocity ( $V_e$ ). This extra velocity changes the speed of the

spacecraft while in heliocentric orbit around the Sun. Given the proper velocity a body goes into a heliocentric solar orbit that carries it to the destination planet along its new elliptical path. To reach the outer planets a spacecraft must be launched fractionally faster than the planetary escape velocity ( $V_e$ ) and must be launched in the same direction the Earth moves around the Sun. The extra fractional velocity ( $dV$ ) then adds to the 29.73 km/sec the spacecraft has because of the Earth's heliocentric motion around the Sun ( $V_{cs}$ ). The spacecraft's final speed around the Sun ( $V_1 = dV + V_{cs}$ ) causes it to coast outward until it reaches the outer planet.

For small body orbiting another, very much larger body (such as satellite orbiting the earth), the total energy of the body is just the sum of its kinetic energy and potential energy, and this total energy also equals half the potential at the average distance  $a$ , (the semi-major axis):

$$E = \frac{1}{2} m v^2 - \frac{GMm}{r} = \frac{-GMm}{2a}$$

Solving these equations for velocity results in the orbital energy conservation equation,

$$v^2 = \mu \left( \frac{2}{r} - \frac{1}{a} \right)$$

Where:

$v$  is the speed of orbiting body

$\mu = GM$  is the standard gravitational parameter of the primary body

$r$  is the distance of the orbiting body from the primary focus

$a$  is the semi-major axis of the body's orbit

Therefore the delta-v required can be computed as follows

$$\Delta v_1 = \sqrt{\frac{\mu}{r_1}} \left( \sqrt{\frac{2r_2}{r_1+r_2}} - 1 \right)$$

$$\Delta v_2 = \sqrt{\frac{\mu}{r_2}} \left( 1 - \sqrt{\frac{2r_2}{r_1+r_2}} \right)$$

Where  $r_1$  and  $r_2$  are, respectively, the radii of the departure and arrival circular orbits, the total  $\Delta v$  is then:

$$\Delta v_{total} = \Delta v_1 + \Delta v_2$$

By Kepler's third law, the time taken to transfer between the orbits is:

$$t_H = \frac{1}{2} \sqrt{\frac{4\pi^2 a_H^3}{\mu}} = \pi \sqrt{\frac{(r_1+r_2)^3}{8\mu}}$$

To reach an inner planet (i.e. Mercury), a spacecraft must be launched from Earth at a velocity greater than the planetary escape velocity ( $V_e$ ). This extra velocity changes the speed of the spacecraft while in heliocentric solar orbit around the Sun. Given the proper velocity a body goes into a solar orbit that carries it to the destination planet along its new elliptical path. To reach the outer planets a spacecraft must be launched fractionally faster than the planetary escape velocity

( $V_e$ ) and must be launched in the opposite direction the Earth moves around the Sun. The extra fractional velocity ( $dV$ ) then subtracts from the 29.73 km/sec the spacecraft has because of the Earth's heliocentric motion around the Sun ( $V_{cs}$ ). The spacecraft's final speed around the Sun

( $V_1 = V_{cs} - dV$ ) causes it to coast inward until it reaches the inner planet.

#### Input and Output Data

- 1) Destination planet for heliocentric Transfer - Select Mercury, Venus, Moon, Mars, Jupiter, Saturn, Uranus, Neptune, or Pluto as the destination planet.
- 2) True anomaly at origin planet, Earth ( $V_1$ ) - Angular position (deg) of the spacecraft at burnout (T-1) in Earth orbit.
- 3) True anomaly at destination planet ( $V_2$ ) - Angular position (deg) of the spacecraft at point of intersection (T-2) with orbit of the destination planet.
- 4) Burnout altitude at origin planet, Earth ( $H_b$ ) - Altitude (M, FT or DU) of the spacecraft at burnout (T-1) in Earth orbit.
- 5) Destination planet misses distance (X) - Intersection point on the destination planet's orbit in front (+) of or behind (-) the destination planet. Miss distance in units of kilometers (KM), nautical miles (N.MI) or Canonical units (DU = Earth radius).

On the Trajectory plot a red curve indicates the spacecraft's trajectory as it travels along its elliptical path to the destination planet. T-1 on the origin planet's orbit indicates the spacecraft's

position at burnout above the Earth. T-1 on the destination planet's orbit indicates the destination planet's position when the spacecraft is first inserted into its elliptical orbit. T-2 on the origin planet's orbit indicates the Earth's position when destination planetary encounter occurs and T-2 on the destination orbit indicates the destination planet's position at time of planetary encounter with a spacecraft from Earth.

The burnout altitude chosen was 300km for all the attempts to get the minimum amount of time to get to Mars. The two driving factors for this trajectory design were anomaly angles at origin and destination planet. Different anomaly angles were taken for both destination and origin planets. Few attempts were made by changing the angles as shown in figures below. The destination planet miss distance is taken as 0 as our goal is to land on Mars.

Figure 10 Attempt with anomaly angles 0 & 110 degrees

Figure 10 shows the first attempt with anomaly angles of 0 degree and 110 degrees at Earth (origin) and Mars (destination) planets respectively. This attempt gives the time of 134 days from burnout to intercept.

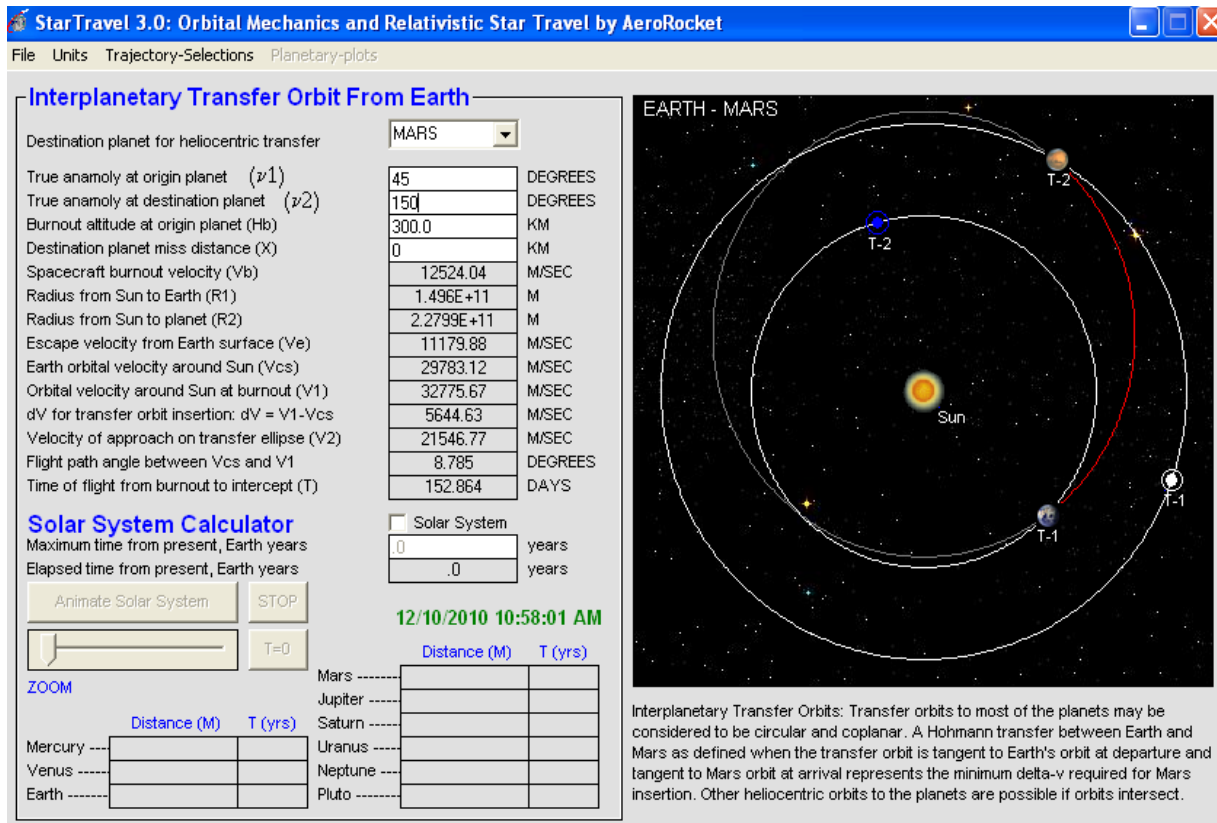


Figure 11 Attempt with anomaly angles 45 & 150 degrees

Figure 11 shows the attempt with anomaly angles of 45 degrees and 150 degrees at Earth (origin) and Mars (destination) planets respectively. This attempt gives the time of 152 days from burnout to intercept. Several attempts were made with different anomaly angles ranging from 0 to 180 for origin and destination planet.

Figure 12 shows the attempt with anomaly angles of 39 degrees and 81 degrees at Earth (origin) and Mars (destination) planets respectively. This attempt gives the time of 47 days from burnout to intercept. Figure 13 shows the attempt with anomaly angles of 60 degrees and 91 degrees at Earth (origin) and Mars (destination) planets respectively. This attempt gives the time of 39 days from burnout to intercept.

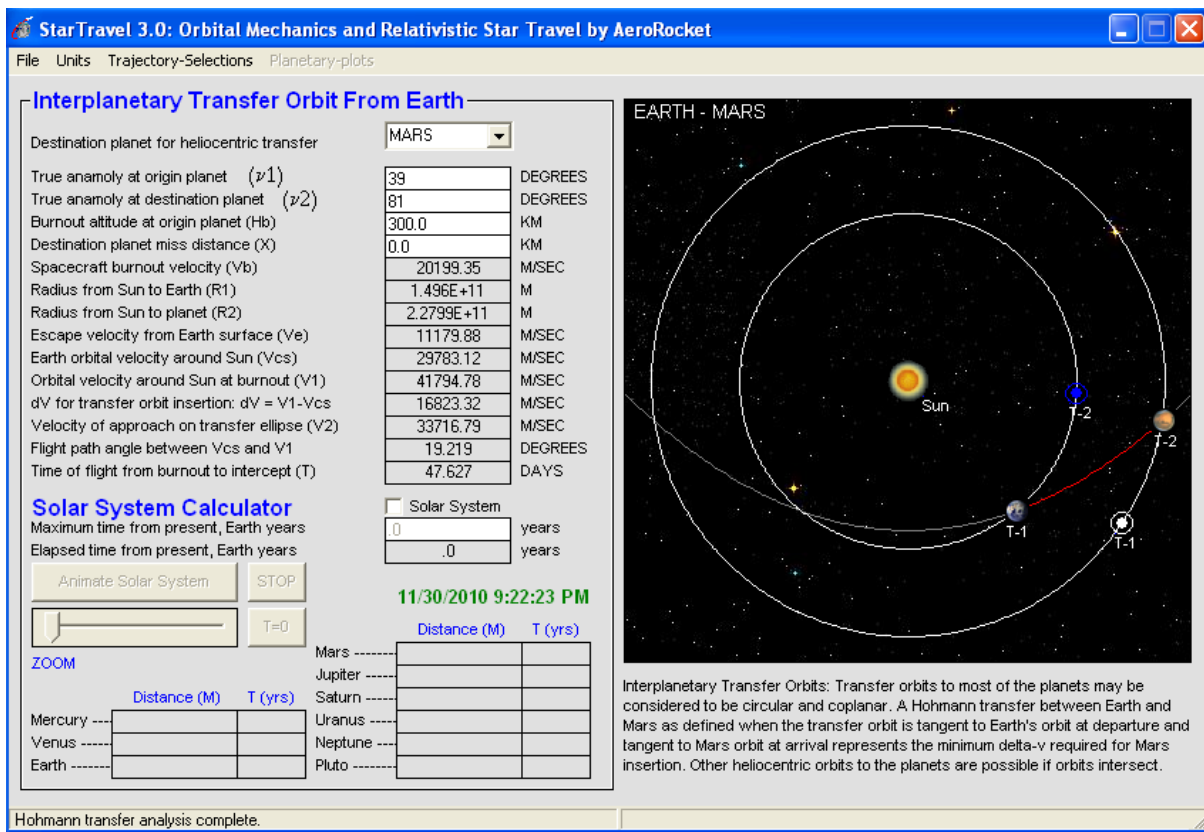


Figure 12 Attempt with anomaly angles 39 & 81 degrees

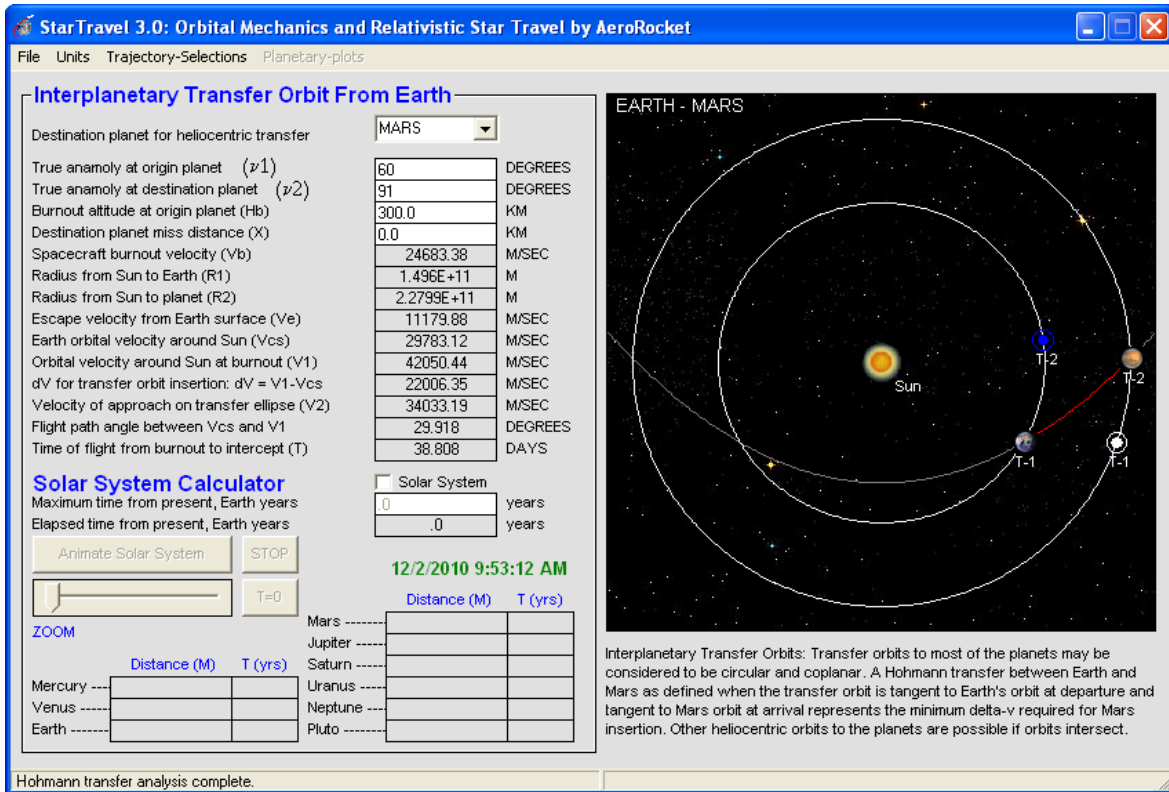


Figure 13 Attempt with anomaly angles 60 & 91 degrees

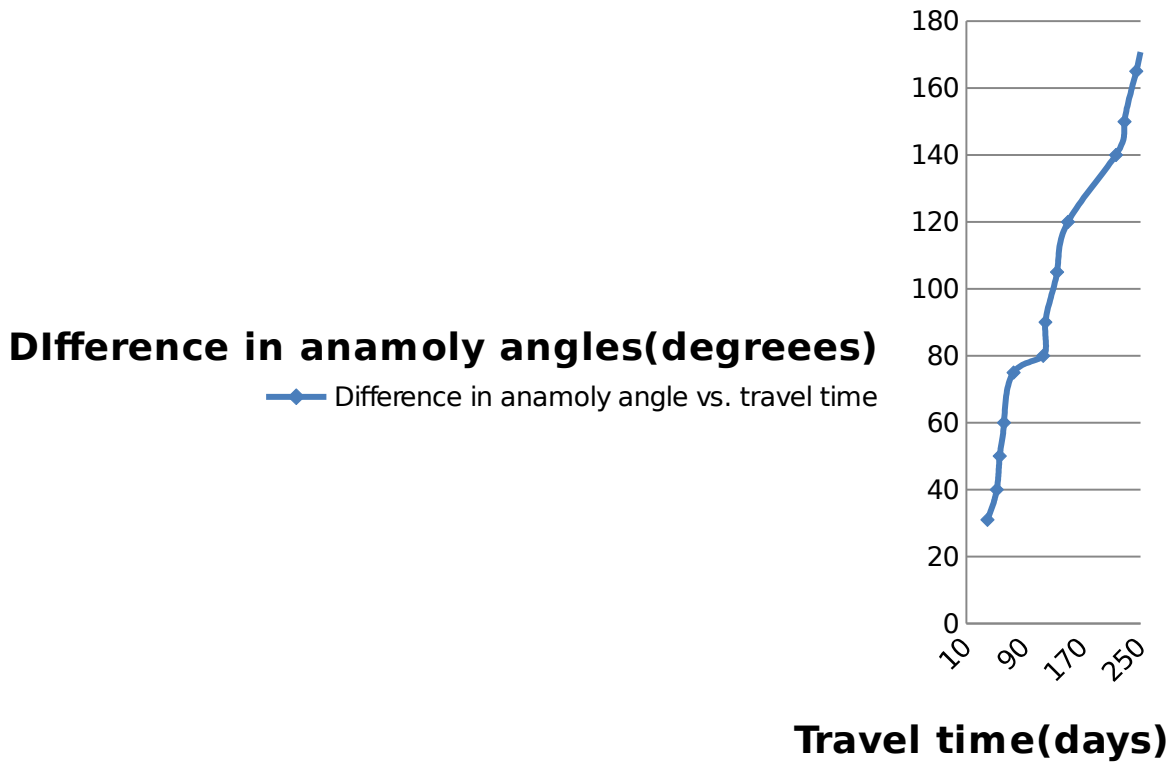


Figure 14 Difference in anomaly angles vs. Travel time

Figure 14 shows the difference in anomaly angles vs. travel time in days. It shows the how the effect of difference of origin and destination planet anomaly angles on the travel time of the spacecraft from the burnout to the intercept.

Table 3 below shows the requirement to meet the objective of reaching Mars in 39 days. It is calculated by one module of the Star Travel software. The latest development allows us to use the power of 200kW for each VASIMR engine which gives an  $I_{sp}$  of 5000 sec. Initial mass of the s/c is 34.7 tone.

Table 3 Calculated parameters

<b>VASIMAR thrust and power requirements</b>	<b>Values</b>
Burn time required	39 days
Input power for each plasma rocket	200 kw
Specific impulse for each plasma rocket	5000 sec
Initial mass of the s/c before burn at insertion	34.7 tone
Thrust of each VASIMR	5 Newton
Total no. of VASIMR motor required	45
Orbital velocity of Earth around the Sun	29.78 km/s
Total power required	9 mw
Total thrust generated	225 newton
Ideal exhaust velocity achieved by VASIMR	51.18 km/s

Total propellant mass	15462.24 kg
Delta V	21.403 km/s

Total  $V = dV + V_{cs} = 21.40 + 29.78 = 51.18$  km/s, Whereas, Star Travel gives total  $V$  of  $22 + 29.78 = 51.78$  km/s and burn time of 38.80 days. The understanding of how the start travel works is explained in the beginning section of this chapter.

## 4.0 VASIMR engine

### 4.1 Selection of propellant

There are four different possible propellant gases which can be used for the specific mission. These four gases can be converted to plasma at given conditions.

Table 4 Propellant properties and parameters

Propellant	Argon(Ar)	Xenon(Xe)	Hydrogen(H)	Neon(Ne)
<b>Properties</b>				
Atomic Weight	39.948	131.3	1.0079	20.179
Atomic Volume(cm <sup>3</sup> /mol)	22.4	37.3	14.4	16.7
Density @293K(g/cm <sup>3</sup> )	0.001784	0.00588	0.0000899	0.0009
State	gas	gas	gas	gas
Melting Point (K)	83.85	161.3	14.01	24.53
Boiling Point (K)	87.3	165	20.28	27.1
Specific Heat Capacity(J/gK)	0.52	0.158	14.304	0.904
Heat of vaporization(kJ/mol)	6.447	12.636	0.904	1.7326
Heat of fusion(kJ/mol)	1.188	2.297	0.117	0.3317
1st Ionization Energy(kJ/mol)	1520.5	1170.4	1312	2080.6
2nd Ionization Energy(kJ/mol)	2665.8	2046.4	-	3952.2
3rd Ionization Energy(kJ/mol)	3930.8	3097.2	-	6121.9
Thermal Conductivity(W/mK)	0.0177	0.00565	0.1805	0.05
Cost in \$ (/100g)	0.5	120	12	33
Ionization Energy/Cost (eV)	100	80	200	150

Argon, Neon, Hydrogen and Xenon are the possible gases that can be used. Different properties and parameters are as shown in the table above. After seeing and considering all the possible properties of all gases it seems that any of the above listed gas can be used. The major concern in this kind of rocket design projects is cost and weight. As it is shown in the table the cheapest available gas is argon. Argon is about \$40/kg vs. Xenon about \$2000/kg. Argon is used for the proposed mission here.

## 4.2 Injector

Injector is one of the most important parts of the engine as the process of engine start from it. Moog type flow controller is used here to control the flow and from the tank. It is used as an injector which can give propellant flow rate of up to 150mg/s.

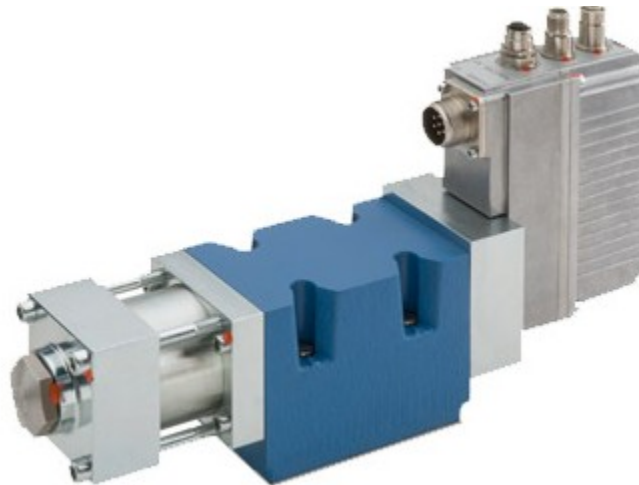


Figure 15 Moog type flow controller Source: <http://www.moog.com/images/Products/>

It can give specific performance as below:

Rated flow: 5 to 100 liters/min

Maximum flow: 180 liters/min (47 g/minute = 783 mg/sec)

100% step response: in 8 ms @ 3,000 psi

The moog type flow controller gives outlet flow in the radius of about 1-4 cm.

### 4.3 Helicon Stage

The helicon stage is the stage where actual propulsion starts of the engine. It gives high temperature to the gas passing in the vacuum space between the two ends of the coils. The helicon is a helical antenna with the width of 11 cm spread over the length of 16 cm.



Figure 16 Steady-state helicon discharge Source: Blackwell, 1997

A very high quality glass tube is inserted in the helicon antenna which can bear the high temperatures. Figure18 below shows the radial profile of temperature and density for the helicon stage at two different magnetic field strength values. 0.084T and 0.11T are the two different magnetic field strengths used shown in the unit tesla. The glass tube in between is made of 4 cm in diameter as it gives the possibility of the lowest operating temperature. Ion density is shown in the power of 22 whereas the temperature measurements are in the eV. Figure 17 below shows

the actual helicon antenna when mounted and to be used in VASIMR engine test. It shows the helicon antenna mounted in the open space between the magnetic mirrors.



Figure 17 Actual Helicon antenna Source: Baity, 2003

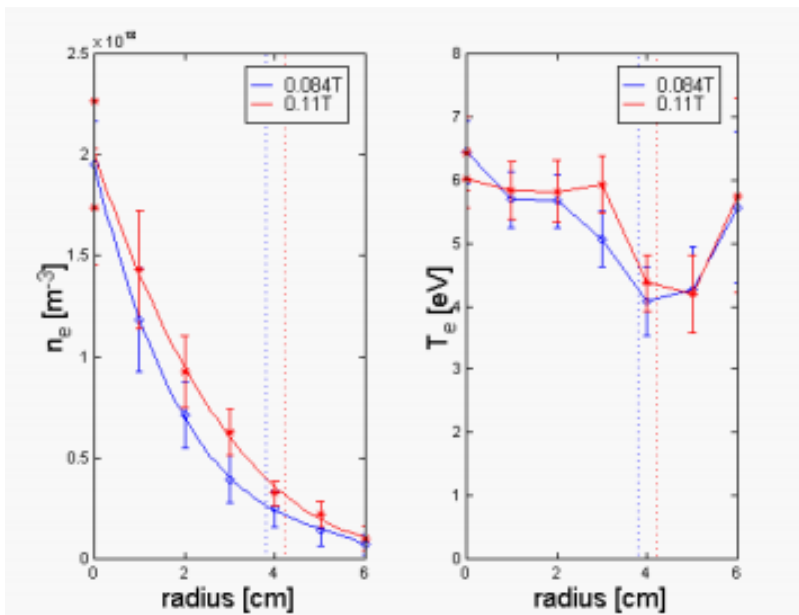


Figure 18 Profiles of density and temperature Source: Baity, 2003

The helicon stage is operated at 30 kW power. In this stage the argon gas is heated such that plasma is generated in this stage. The cold plasma travels through the engine and reaches to the ICRH part of the engine.

#### 4.4 ICRH (Ion Cyclotron Resonance Heating)

ICRH is the stage where the plasma gets heated to maximum temperature and will be exhausted out through the nozzle to get the thrust. The ions or plasma is heated up to the cyclotron frequency which is the frequency of a charged particle moving perpendicularly to the direction of a uniform magnetic field, i.e. a magnetic field of constant magnitude and direction. Since that motion is always circular, the cyclotron frequency is well defined. This portion of the engine works at 160 to 170 kW of electric power.

ICRH uses antenna like one used in helicon stage. The structure and dimensions depend on their efficiency. It has a width of 11 cm and length of 20 cm. According to the recent improvement the most efficient ICRF antenna can give 66% of efficiency with 0 degree twist in the antenna structure. (Glover, 2010)

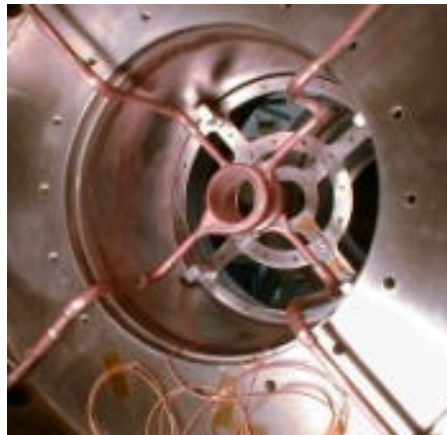
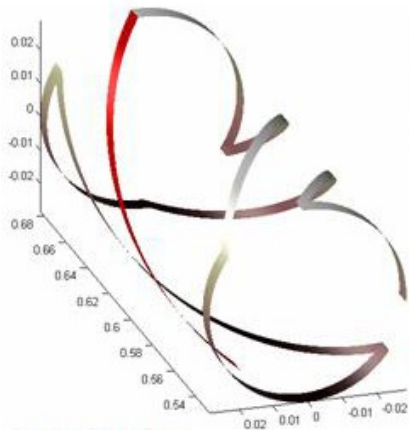
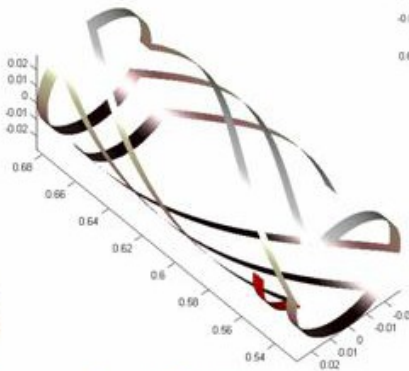


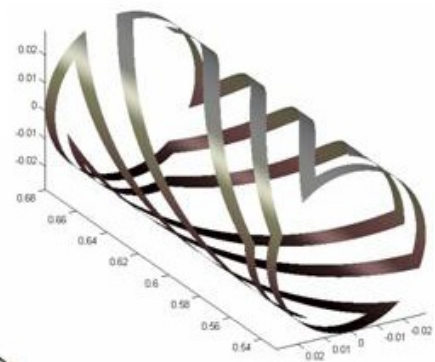
Figure 19 Actual ICRH antenna Source: Bering, 2006



**Double Strap**  
 Half Twist Antenna:  
 Ion loading **70 mΩ**  
 Electron loading **50 mΩ**  
 ICRF efficiency **38%**  
 Ion power fraction **58%**



**Triple Strap**  
 Half Twist Antenna  
 Ion loading **138 mΩ**  
 Electron loading **96 mΩ**  
 ICRF efficiency **54%**  
 Ion power fraction **59%**



**Quadruple Strap**  
 Half Twist Antenna  
 Ion loading **149 mΩ**  
 Electron loading **197 mΩ**  
 ICRF efficiency **63%**  
 Ion power fraction **43%**

# ICRF antenna improvement

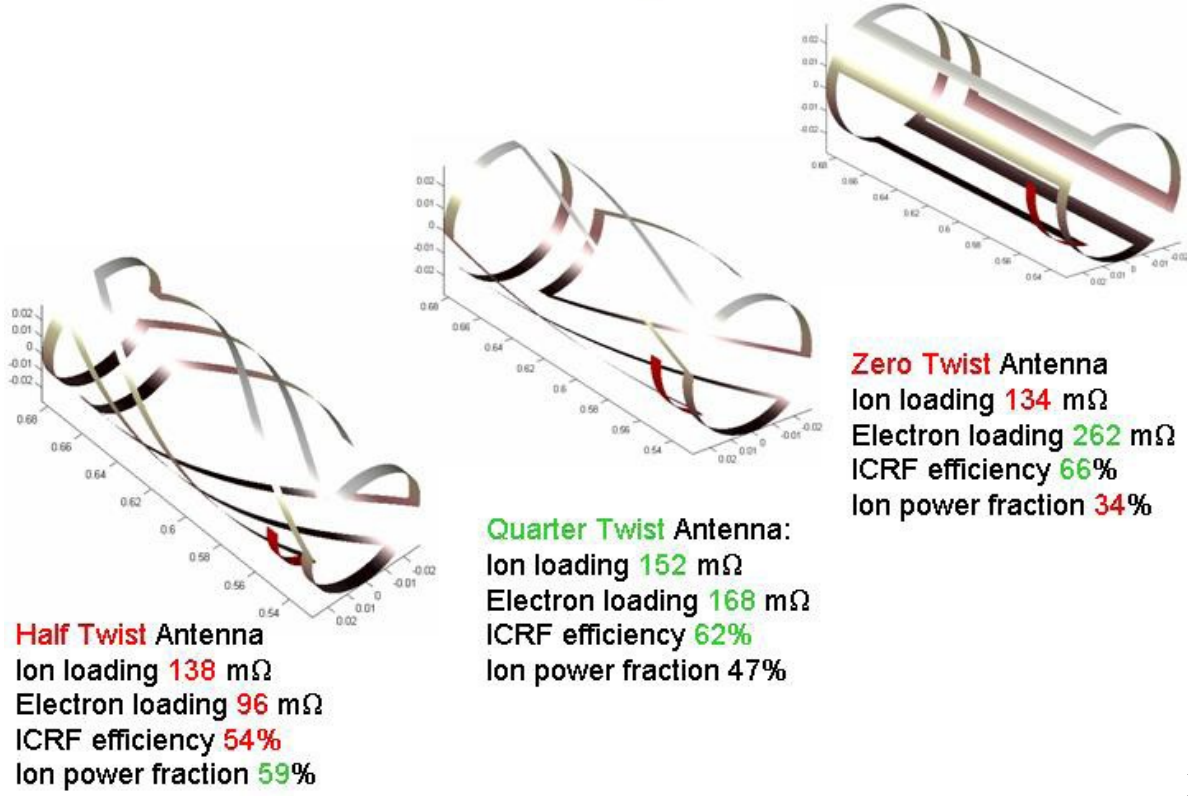


Figure 20

re 20 ICRF antenna improvement Source: Ilin, 2003

Figure 19 shows the actual ICRH antenna used in the VASIMR engine test. Figure 20 shows possible different possible geometry for the ICRH antenna. Each of them was tested and subjected to get the maximum efficiency by using different input parameters. It is compared in the table below which shows the maximum efficiency achieved was 66% with no twist in the antenna geometry.

Table 5 ICRH performance for different configuration

Antenna Geometry	Ion Loading	Electron Loading	Ion Power fraction	Efficiency (%)
Double Strap, half twist	70	50	58	39
Triple Strap, half twist	138	96	59	54
Quadruple Strap, half twist	149	197	43	63
Half twist	138	96	59	54
Quarter twist	152	168	47	62
Zero twist	134	262	34	66

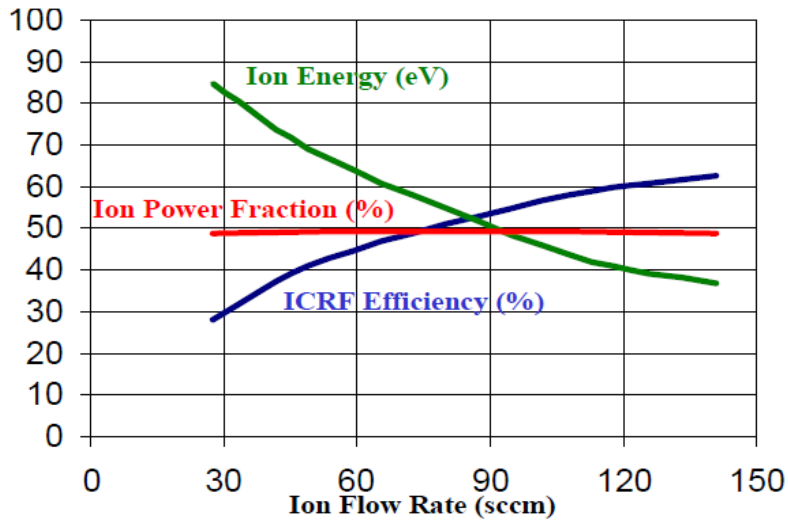


Figure 21 ICRF performance dependence on the input ion flow rate Source: Ilin, 2003

Extensive parameter studies are being conducted at the ASPL to optimize ICRF heating performance. Figure 21 demonstrates the effect of ion flow rate on ICRF efficiency and ion power fraction, by EMIR simulation for plasma. The plasma density was fixed, while the input flow velocity was varied. As shown in Fig. 21, the ICRF efficiency goes up with the ion flow velocity, while the ion power fraction does not change much.

#### 4.5 Magnetic Mirror

Use of hot plasma in the engine requires strong confining magnetic fields, which can withstand the very high temperatures during the operational periods of the engine. Other important requirement is that the magnetic field must be produced in the light weight and compact systems with virtually no loss of power. BSCCO (Bismuth Strontium Calcium Copper Oxide), is the high power superconducting compound is the best choice for the VASIMR high temperature operating environment. Current study on  $MgB_2$  (Magnesium diboride) implies that it could be a good replacement for the BSCCO as it is less expensive and easily manufactured. The thermal cooling can be done by using existing cryocooler technology, or use of cryogenic propellant (deuterium or Hydrogen) can handle much of the cooling requirements. The currently used BSCCO magnet is an 8 superconducting pancake set, assembled under an axial compression load. It is made of approximately 500 turns and a current passing through 110 amps and is able to produce a magnetic field up to 3 tesla.

#### **4.6 Magnetic Nozzle**

The magnetic nozzle serves to direct and expand the plasma flow, increasing its directed axial energy and minimizing plume impingement on the surrounding spacecraft structure. In

order for the magnetic nozzle to have any effect, the plasma must be magnetized. This means conceptually that the applied magnetic field is sufficiently strong to hold ions and electrons in orbits around the axial field. The theory of magnetic nozzle is still in the early stage and poorly understood. The conventional nozzle half angle theory is expected to be true in the case of magnetic nozzle. Therefore the best half angle for nozzle was

chosen 15 degrees. The lack of detailed information on parameters at different sections does not allow calculating the actual derivation of dimensions of the nozzle. Estimated nozzle dimensions were used to continue the design.

#### **4.6 Drawings**

After collecting information from the ADAstra Rocket Company, articles and technical papers on VASIMR, technical papers and publications on the different parts of the engine and their development, and applying engineering approximation leads to the specific part design and the overall engine dimensions as shown below in the drawings. Solid works has been used to draw the different part and assemble them to make a complete geometry of the engine.

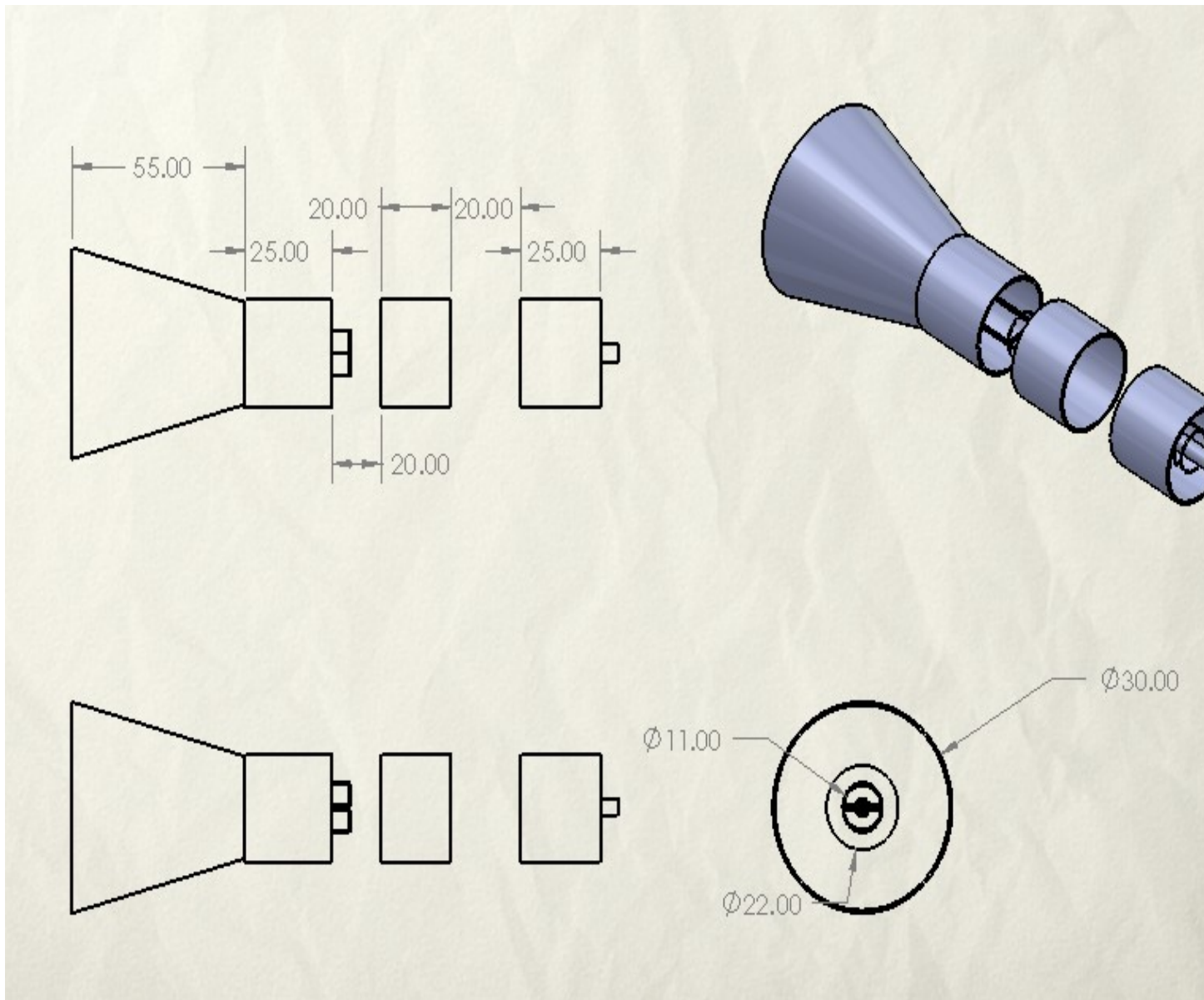


Figure 22 VASIMR Engine Solid works 3D drawing

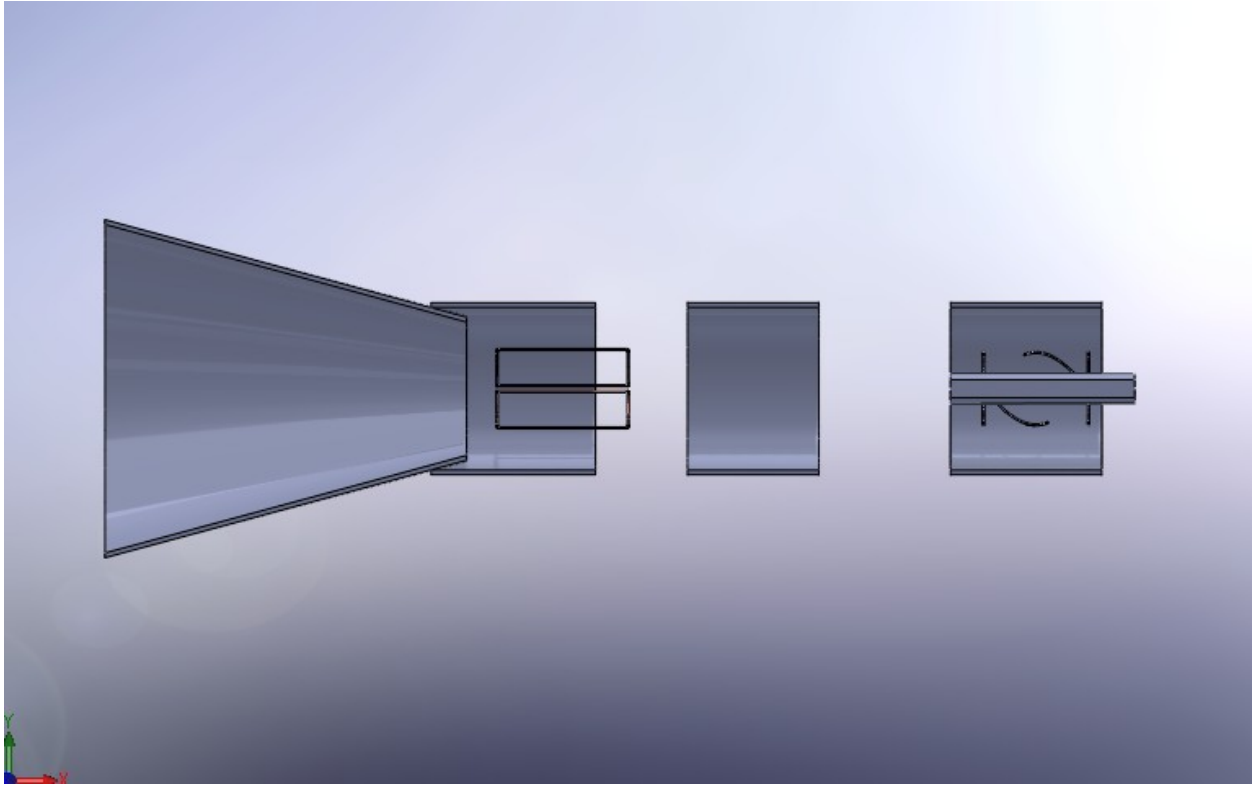


Figure 23 VASIMR side view

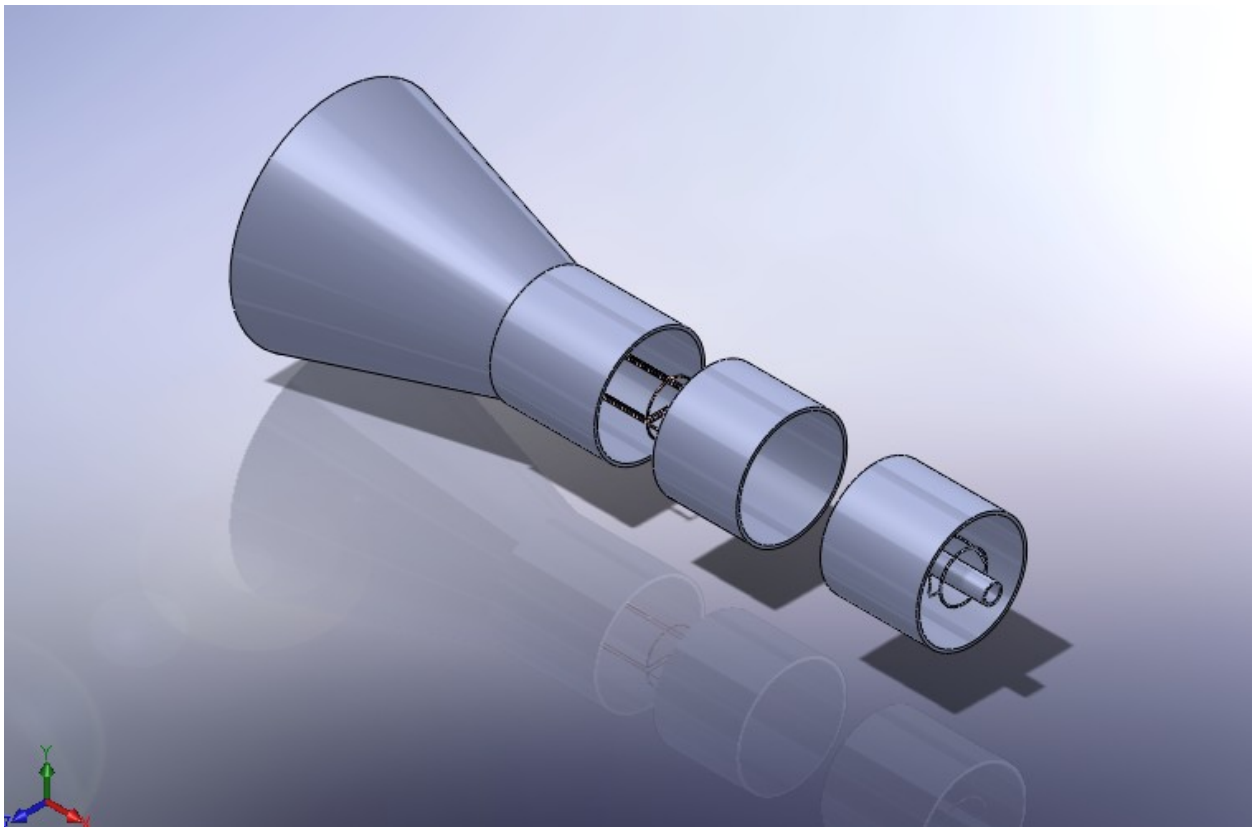


Figure 24 VASIMR engine 3D view

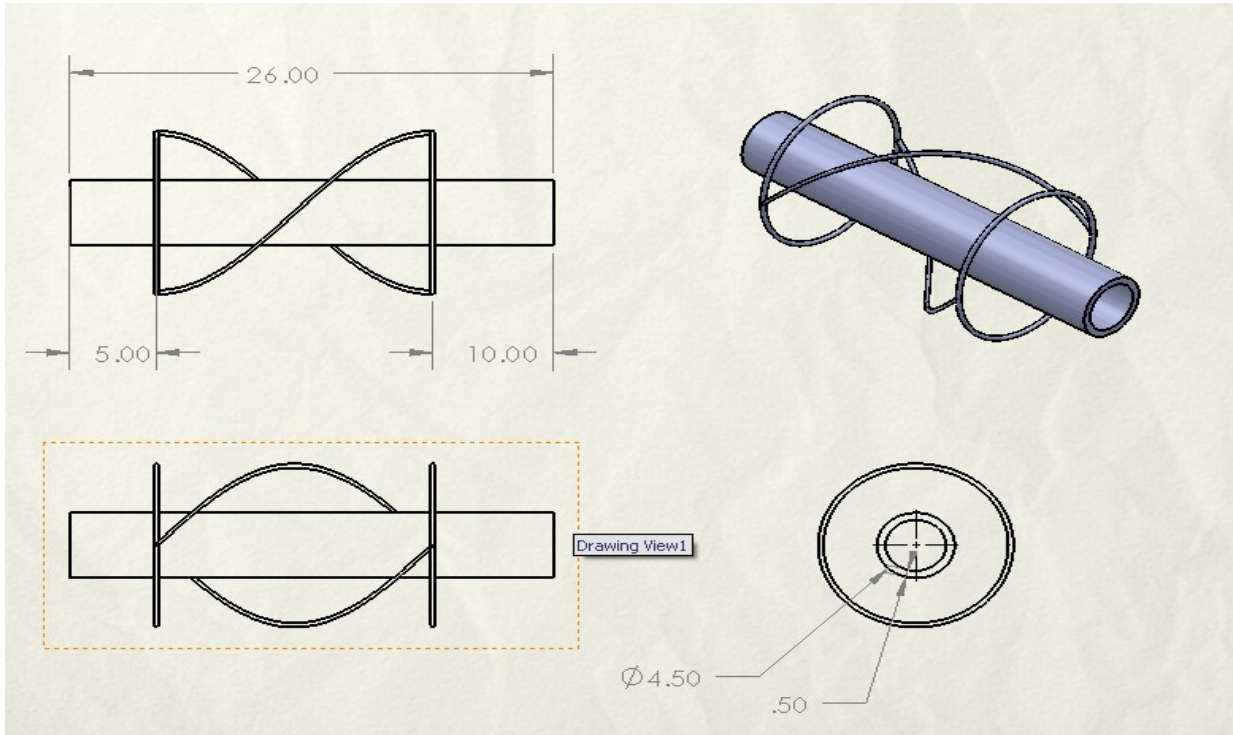


Figure 25 Helicon antenna Drawing

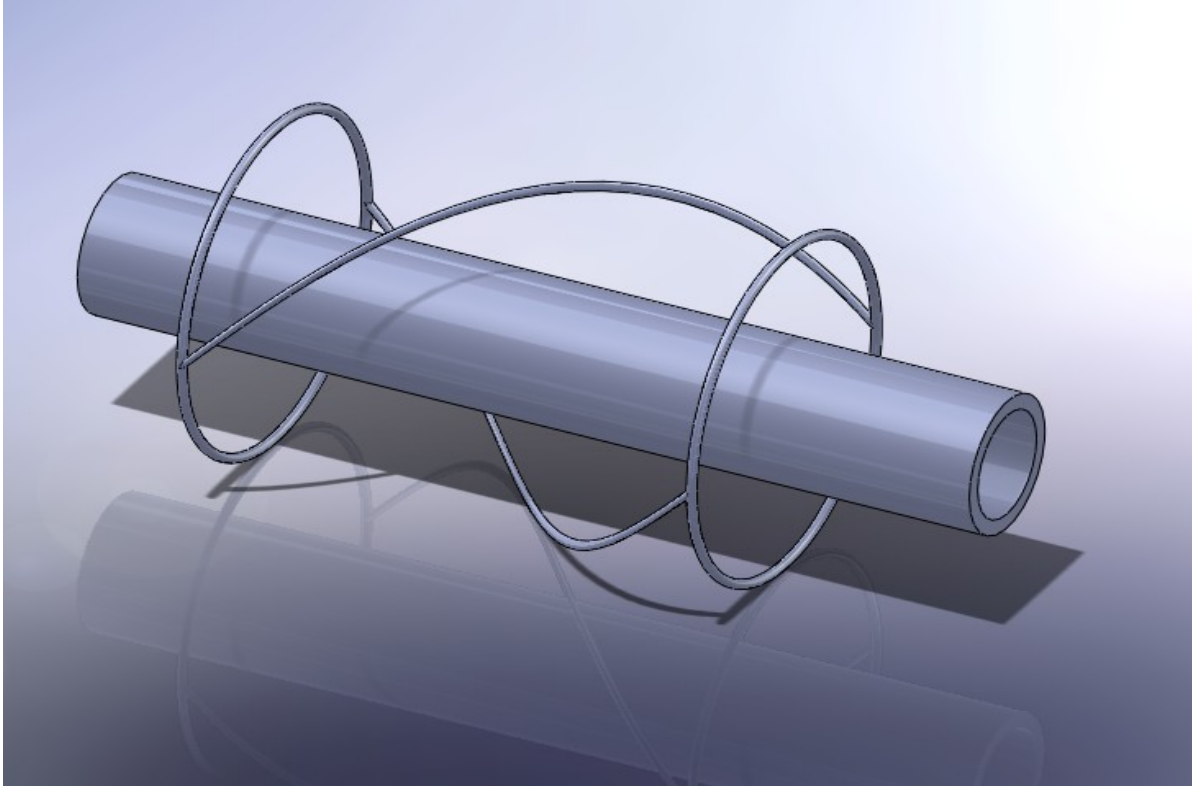


Figure 26 Helicon antenna 3D view

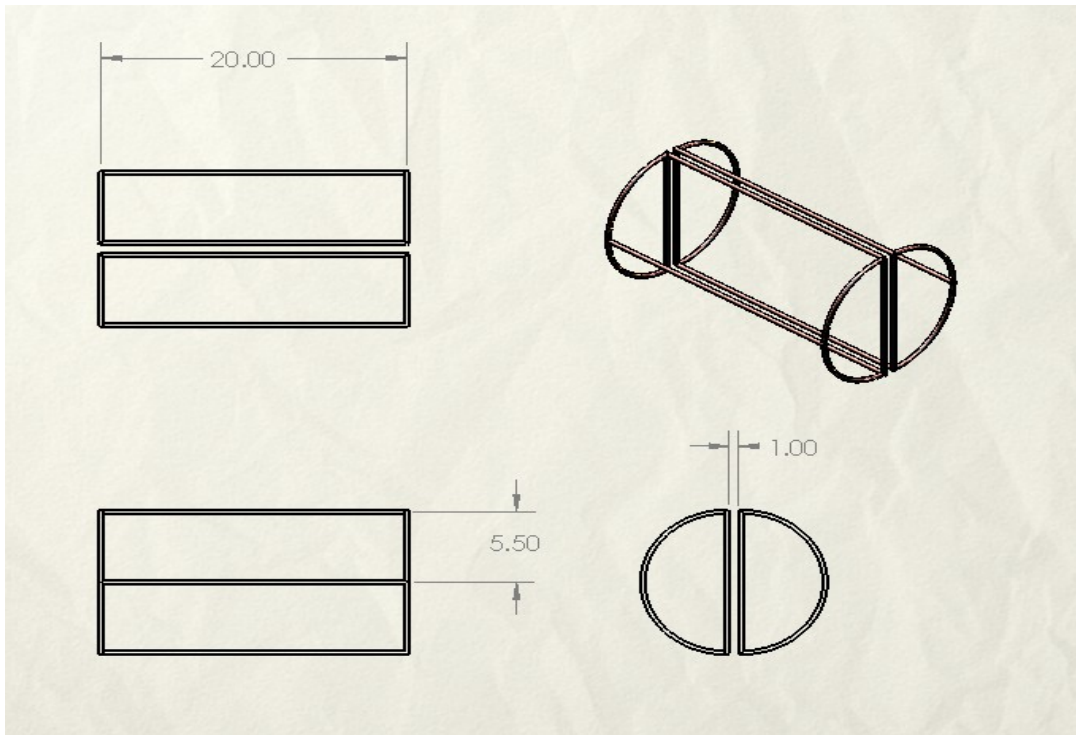


Figure 27 ICRH antenna Drawing

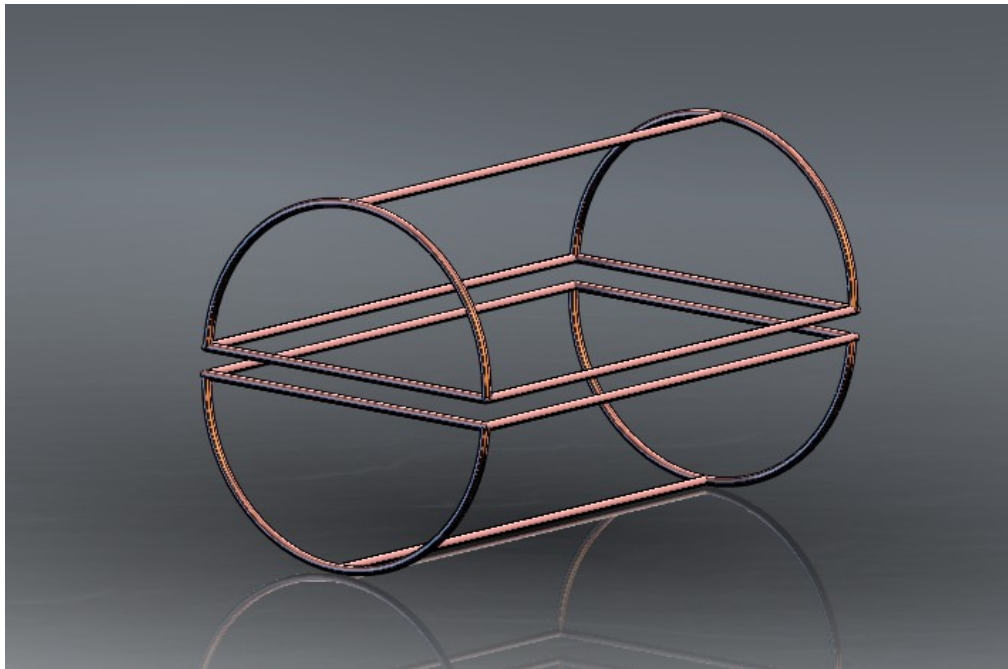


Figure 28 ICRH 3D vie

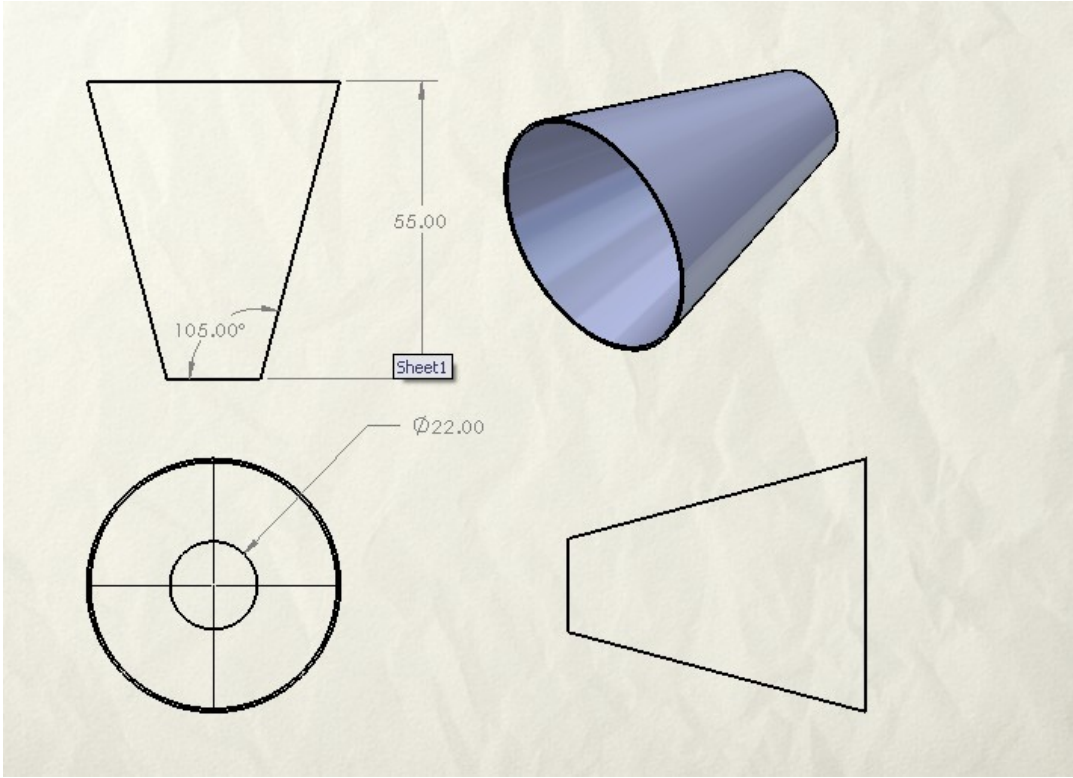


Figure 29 Nozzle drawing

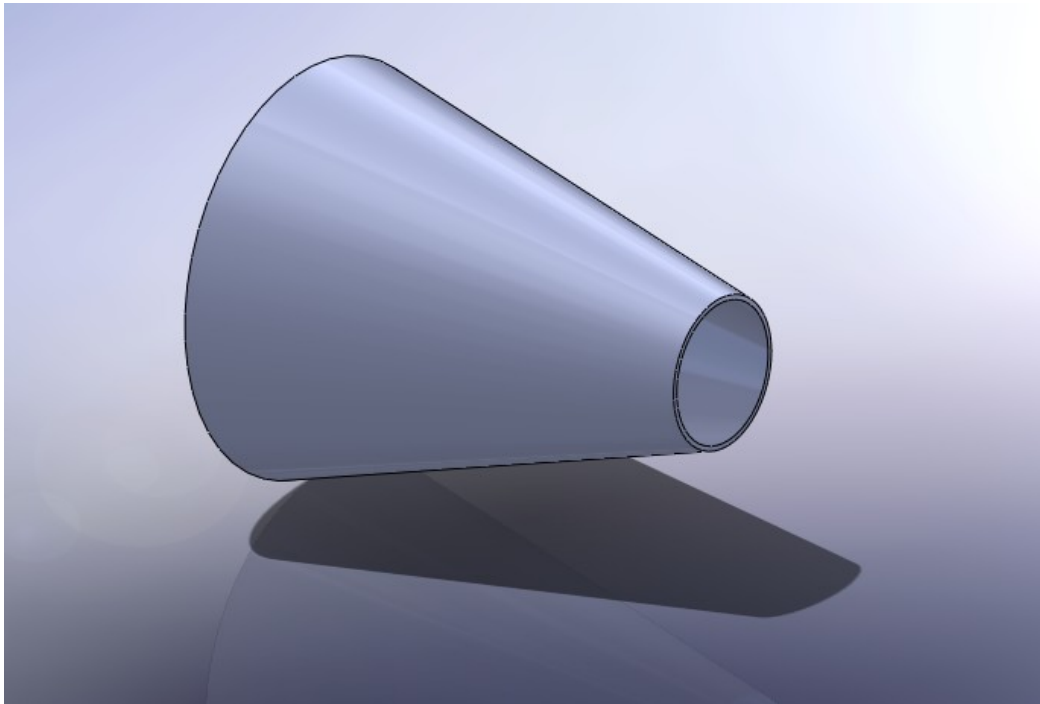


Figure 30 Nozzle 3D view

## 5.0 VASIMR Performance

High-power electric propulsion systems have the capability of reducing the propellant mass for heavy- payload orbit raising missions and cargo missions to the moon and can even reduce the trip time of piloted planetary missions. The Variable Specific Impulse Magnetoplasma Rocket (VASIMRR) is one of the few electric propulsion devices capable of processing great power densities ( $6 \text{ MW/m}^2$ ) with an expected long lifetime. The advantages of the VASIMR are high power, high specific impulse, constant power variable specific impulse, and potentially long lifetime due to the magnetic confinement of the plasma stream. The rocket relies on efficient plasma production in the first stage using a helicon plasma source. Ion cyclotron resonance

enables efficient ion heating in the second stage (RF booster). Thrust is realized in the final stage as the plasma accelerates in a magnetic nozzle.

## 5.1 Measurement of ionization Cost

A key factor in maximizing the overall rocket efficiency is to create the plasma in the first stage with as little power as possible. The commonly used term for plasma generation efficiency is ionization cost and is presented as energy per ion in terms of electron volts. The VASIMR helicon section has argon input into the upstream end and it flows to the ICH section. The RF power strips one electron of each ion.

Power is lost through radiation from the excited argon neutrals and ions, flux of plasma to the walls where it recombines, and the frozen flow loss of ionization energy carried out of the helicon section. The ions also carry kinetic energy,  $E_1$ , but we do not count that as a loss since that energy represents thrust. Therefore the ionization cost is given by,

$$E_i = \frac{P_{1,RF}}{\dot{m}} - E_1 \quad (2)$$

$m_{Ar}$

Table 6 Ionization cost relative to Power

$E_i$ (eV)	$P_{1, RF}$ (kW)
151	15
135	16
142	18
128	19
122	20
117	21
109	22
104	23
97	24
94	25
<b>87</b>	<b>28</b>
89	30
93	31
96	32
97	33

99	34
102	35

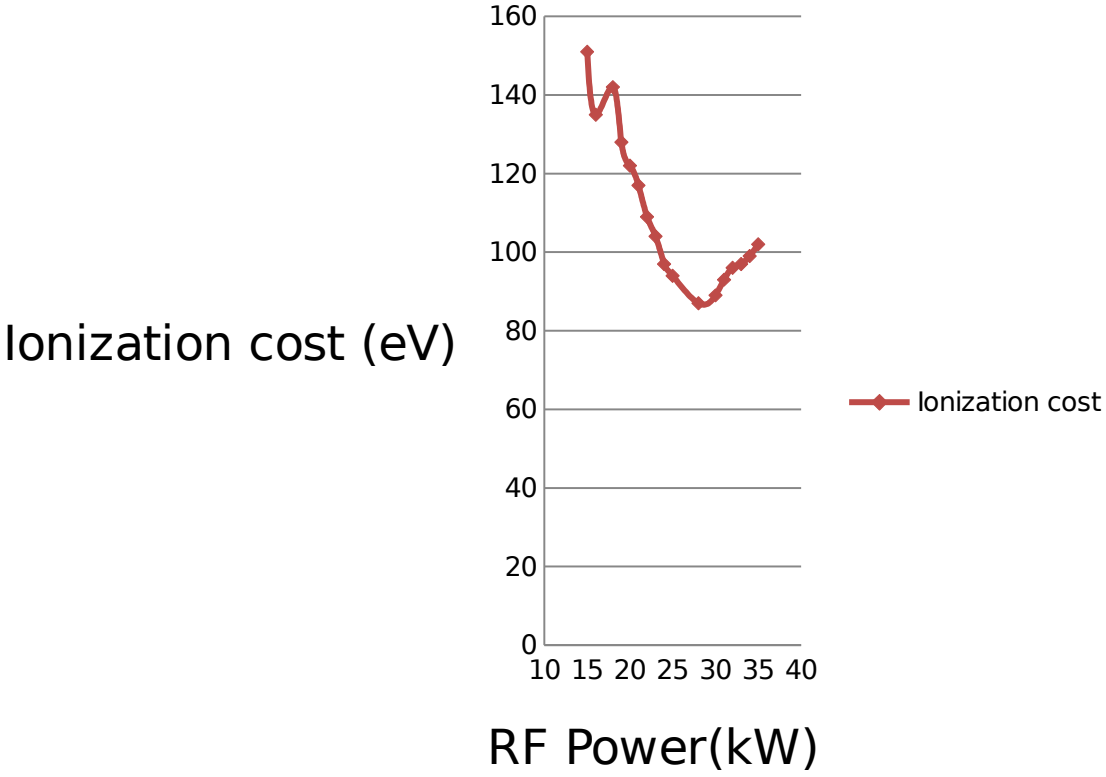


### Figure 31 Ionization cost vs. RF Power

The graph above shows Ionization cost vs. RF Power graph. The RF power used in above graph is only for the helicon stage. Minimum ionization cost is at 28kW of RF power. New measurements of the ionization cost were taken during helicon-only operation as a function of both RF power and argon propellant flow rate within the ranges of 15 to 35 kW and 50 to 150 mg/s, respectively. Ionization cost was determined by measuring the total ion flux from the VX-200 and then dividing the coupled RF power to the plasma by the total ux. Figure 32 is a contour map of the helicon performance as an ion source, and shows a clear indication of a valley of optimum ionization cost, as low as 87eV per ion. (Bering, 2006) Of course, each new core and helicon coupler will produce a unique ion cost performance map; though in general it is clear that providing too much propellant with too little RF power will result in an inefficient helicon plasma source. A scenario where there is too little propellant and too much RF power will also result in an inefficient helicon plasma source. A key point to remember with these ionization cost measurements is that this is the cost of an ion that is actually extracted all the way through the rocket core, which is in many cases quite different from the ion cost directly within a helicon source tube. The lowest ionization cost measurement of 87eV occurred with VX-200 settings of 28 kW and 130 mg/s.

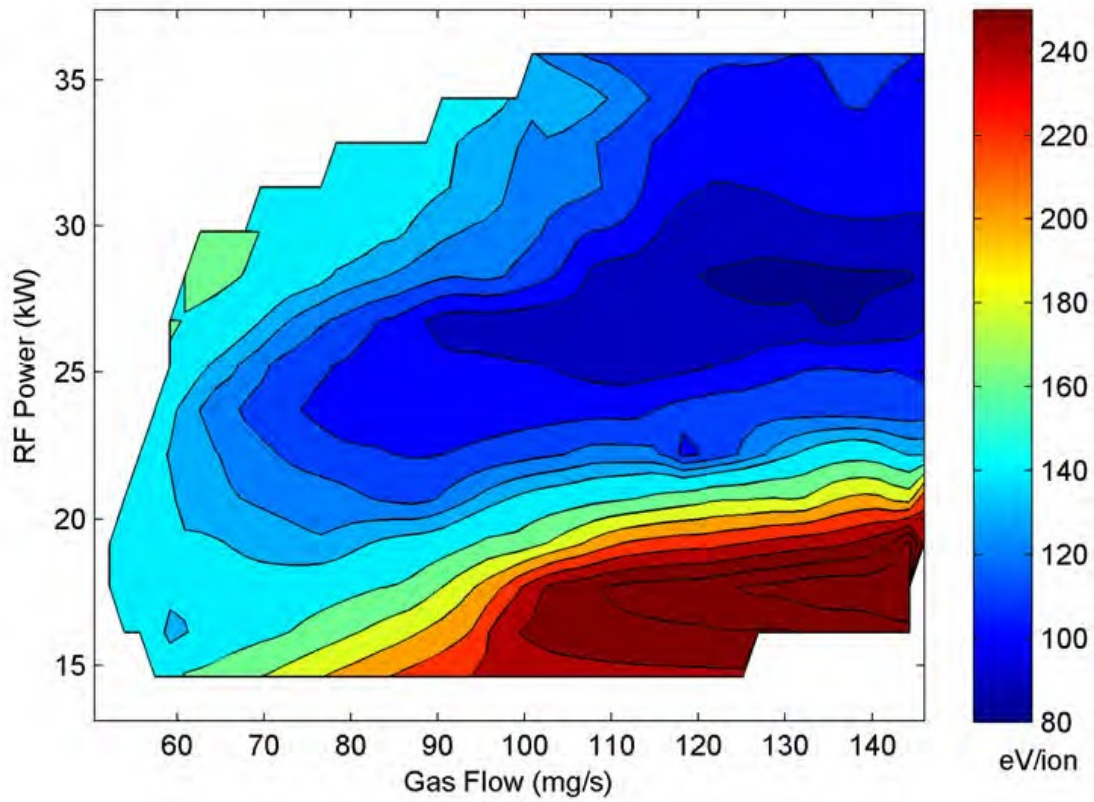


Figure 32 A color contour plot of the ionization cost of the helicon stage Source: Casaddy, 2010

## 5.2 Thruster Efficiency and Force

The VX-200 thruster efficiency is determined by dividing the total RF power coupled to plasma by the thruster jet power. The jet power is defined as

$$P_{jet} = \frac{F^2}{2\dot{m}} \quad (3)$$

where  $F$  is the total force produced by the rocket and  $\dot{m}$  is the total mass flow rate of

propellant. The force from VX-200 was determined by using a force impact target that measured the local force density within the exhaust plume as a function of radial position.

The thruster efficiency is given by dividing the jet power by the coupled total RF power,

$$\eta_T = \frac{P_{jet}}{P_{1,RF} + P_{2,RF}} \quad (4)$$

;where  $P_{1,RF}$  and  $P_{2,RF}$  represent the RF power coupled to the first and second stage plasma, respectively.

An experiment campaign in May of 2010 that used a propellant flow rate of 107 mg/s yielded results that shows a total force of up to 3.6 N and 54% efficiency at a total coupled RF power of 108 kW. The specific impulse was calculated using the total force measurement and a propellant mass flow rate measurement as,

$$I_{sp} = \frac{F}{\dot{m}g} \quad (5)$$

When the latest results used for the calculations it gave the results as:

Using the  $I_{sp}$  of 5000s and  $\dot{m}$  of 130 mg/s. The maximum force up to date that can be produced is 6.37N. That gives  $P_{jet}$  of 156.065kw and the total coupled power of 200kW, which gives the thruster efficiency of 78%.

Graphs in figure 33 are the experimental representations which show the variation in thruster efficiency in change as coupled RF Power and  $I_{sp}$ . The Helicon stage is left at a constant 28 kW, while the ICH stage power is varied from 0 to 81 kW. The limiting factor in the maximum applied RF power to the VX-200 in this experiment campaign was a vacuum pressure limit within the vacuum chamber, where greater RF circuit voltages produced glow or arc discharges which prompted the solid state RF generators to shut down.

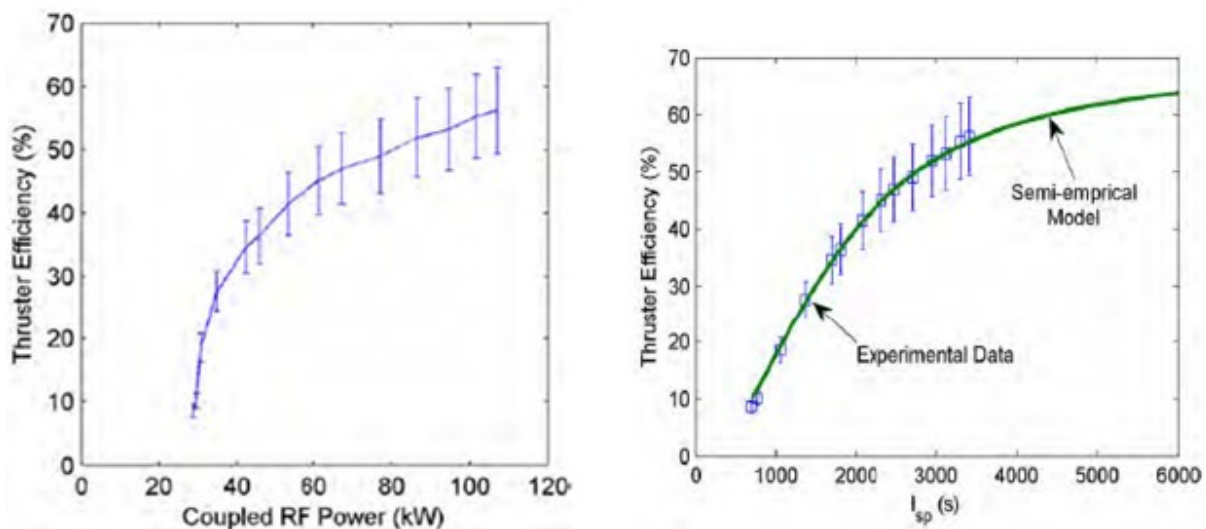


Figure 33 Thruster Efficiency vs. Coupled RF Power and Thruster Efficiency vs.  $I_{sp}$  Source: Cassady, 2010

The efficiency continues to increase as a function of applied ICH RF power, indicating that the process of ICH wave coupling into the plasma column has not saturated.

Table 7  $I_{sp}$ -Force table

<b>mass flow rate (mg/s)</b>	<b><math>I_{sp}</math> (s)</b>	<b>F (N)</b>
130	1000	1.2753
130	1500	1.91295
130	2000	2.5506
130	2500	3.18825
130	3000	3.8259
130	3500	4.46355
130	4000	5.1012
130	4500	5.73885
130	5000	6.3765

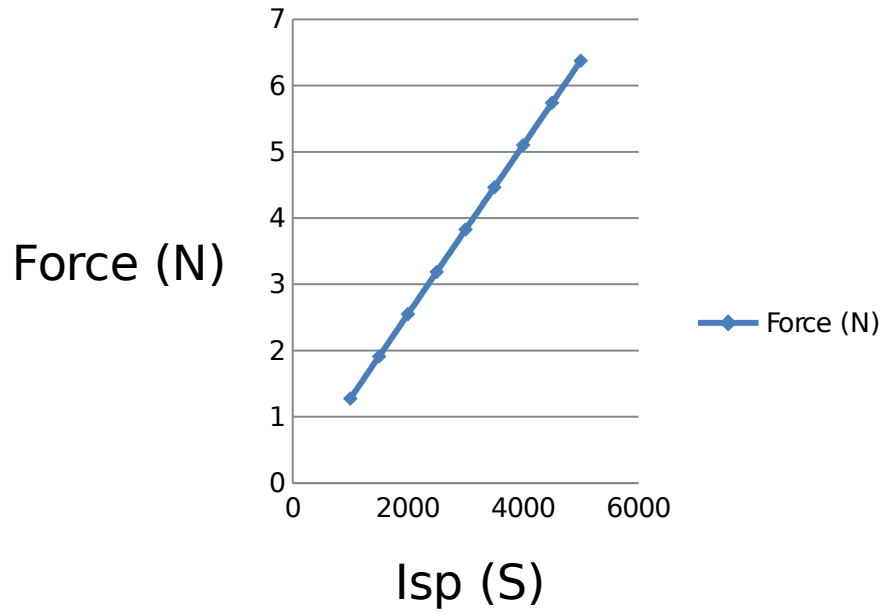


Figure 34 Force vs. I<sub>sp</sub>

Figure 33 also shows the same data set from May 2010 but displays the thruster efficiency of the VX-200 as a function of the specific impulse of VX-200. RPA was used to measure the force at the end on nozzle section. Figure 34 shows the graphical representation of the change in force with I<sub>sp</sub>. Force increases linearly with respect to the increase in Specific Impulse. In figure 34 the I<sub>sp</sub> values are used only up to date development and actually achieved in the test attempts.

### 5.3 Efficiency Model

The thruster efficiency can also be found by using the equations below and thus it can be connected to the other important parameters of the engine.

Power in the helicon stage is,

$$P_{1,RF} = e\Gamma \left( \frac{E_i + E_1}{\eta} \right) \quad (6)$$

RF Power in the ICRH stage is, 
$$P_2 = \frac{1}{\eta_B} e \Gamma E_2 \quad (7)$$

Jet power, 
$$P_{jet} = \frac{1}{2} \Gamma m_{Ar} g^2 I_{sp}^2 = e \Gamma (E_1 + E_2) \eta_n \quad (8)$$

$$E_2 = \frac{\frac{1}{2} m_{Ar} g^2 I_{sp}^2}{e \eta_n} - E_1 \quad (9)$$

Thruster Efficiency, 
$$\eta_T = \frac{P_{jet}}{P_{1,RF} + P_{2,RF}} = \frac{\frac{1}{2} \Gamma m_{Ar} g^2 I_{sp}^2}{e \Gamma (E_1 + E_2 + \frac{1}{\eta_B} E_2)}$$

(10)

$$\eta_T = \frac{\frac{1}{2} m_{Ar} g^2 I_{sp}^2}{e E_1 + e E_1 \left(1 - \frac{1}{\eta_B}\right) + \frac{\frac{1}{2} m_{Ar} g^2 I_{sp}^2}{\eta_B \eta_n}}$$

(11)

Here, the maximum Flux density =  $5.24 \cdot 10^{24}$  tesla

$$P_i = \frac{1}{2} \dot{m}_i (v_{ICRH}^2 - v_{helicon}^2) \quad (12)$$

$$\eta_B = \frac{P_i}{P_{Plasma}} \quad (13)$$

$\eta_B$  is around 36% 49

$P_i$  and  $P_{plasma}$  values are measured in actual experiment.

#### 5.4 Coupling Efficiency

The coupling efficiency for RF antenna power is given by,

$$\eta_A = \frac{R_p}{R_p + R_C} \quad (14)$$

Where,  $R_p$  is plasma resistance and  $R_C$  is the circuit resistance. Coupling efficiency is found to be 0.89. In order to increase the coupling efficiency the plasma resistance should increase and circuit resistance should decrease as much as possible.

The power radiated into the plasma can be found by,

$$P_{Plasma} = \eta_A P_{ICRH} \quad (15)$$

Using the value 170kW for ICRH power, the power radiated into the plasma would be, 1.51 kW.

$$P_{ion} = \Gamma_i W_{ICRH} \quad (16)$$

Obtained ion flux density of  $3.1 \times 10^{20} \text{ s}^{-1}$  and the power given to ion by ICRH was 17 eV gives ion power of 840 w.

$$\eta_{ICRH} = \frac{P_{ion}}{P_{plasma}} \quad (17)$$

Above equation give the ICRH efficiency of 67%.

## 5.5 Nozzle and Magnetic Field

Here the approach of calculating plasma fluid characteristics (density  $n$ , velocity  $V$ , temperature  $T_i$ ) based on the kinetic theory, from the calculated particle trajectories, defined by particle positions and velocities ( $\mathbf{x}$ , and  $v_i$ ) is presented.. The discrete ion density  $n$  is defined constant at each finite difference cell  $X_j$ , using the formula (Cassady, 2010)

$$n(X_j) = w \sum_k \text{Count}(x_k \in X_j) \quad (18)$$

where  $x_k$  is a position of  $k$ -particle,  $w$  is a particle weight calculated, such that it makes the grid density equal given value at given point  $n(X^0) = n^0$ .

Other fluid quantities (velocity  $V$ , ion current density  $j$ , temperature  $T$  and energy  $W$ ) are calculated by a technique similar to that used to calculate the ion density, as presented below: (Cassady, 2010)

$$V(X_j) = \langle \dot{v}_k : x_k \in X_j \rangle = \frac{\sum_k \langle \dot{v}_k : x_k \in X_j \rangle}{\sum_k \text{Count}(x_k \in X_j)} \quad (19)$$

$$j_i = q_i w \sum_k \langle v_k : x_k \in X_j \rangle$$

(20)

$$T_{\parallel}(X_j) = m_i \sum_k \langle (v_{\parallel,k} - V_{\parallel})^2 : x_k \in X_j \rangle / \left( q_i \sum_k \text{Count}\{x_k \in X_j\} \right), \quad W_{\parallel}(X_j) = m_i \sum_k \langle v_{\parallel,k}^2 : x_k \in X_j \rangle / \left( 2q_i \sum_k \text{Count}\{x_k \in X_j\} \right)$$

(21)

Using the equations above for the different geometry points the contour plots were generated by Ilin are showed in the figures below. The figures below respectively shows the 2D plots of plasma density, azimuthal velocity, current velocity, and the magnetic induction along the geometry of the engine.(Ilin, 2005)

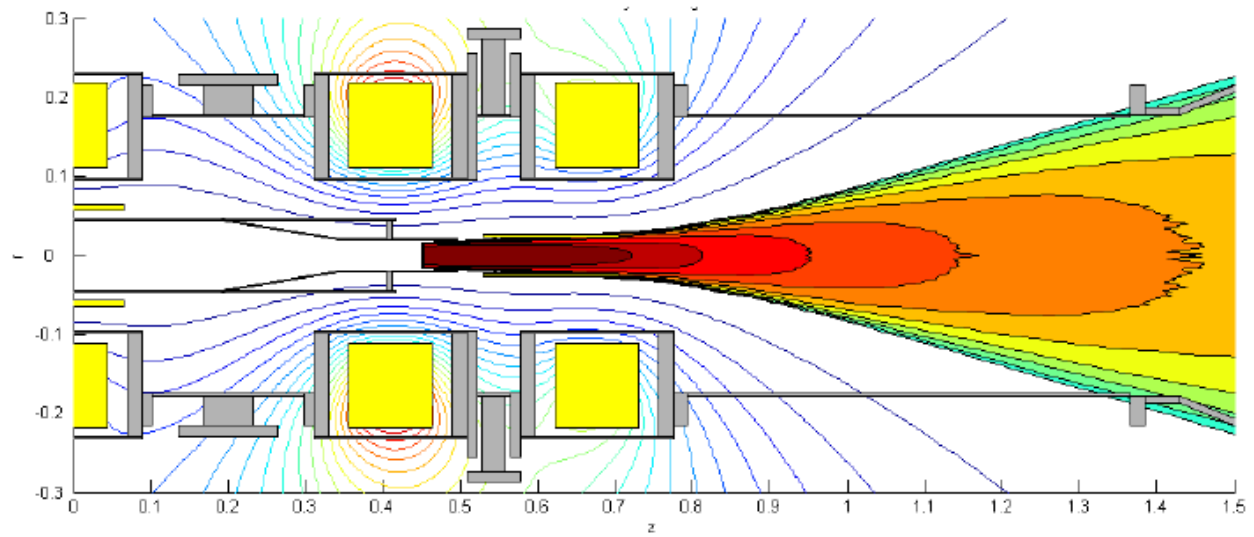


Figure 35 2D contour plot of the plasma density  $n(r,z)$  calculated by the particle trajectory code and magnetic configuration Source: Ilin, 2003

After getting the plasma density calculated by the particle trajectory code, the solution is expanded to the rest of the computational domain using an analytical method.

The first component of the velocity vector is negligible and therefore can be assumed zero on the axis but grows towards the edge of the plasma especially in the area of the antenna as shown in the figure 36.

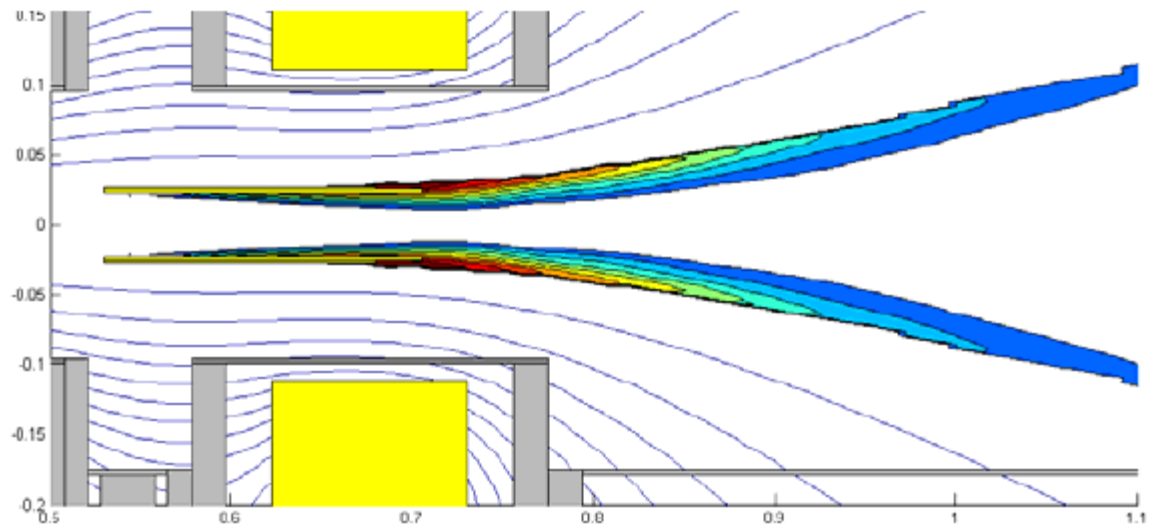


Figure 36 2D contour plot of the plasma azimuthal velocity  $V_{\phi}(r,z)$  calculated by the particle trajectory code and magnetic configuration Source: Ilin, 2003

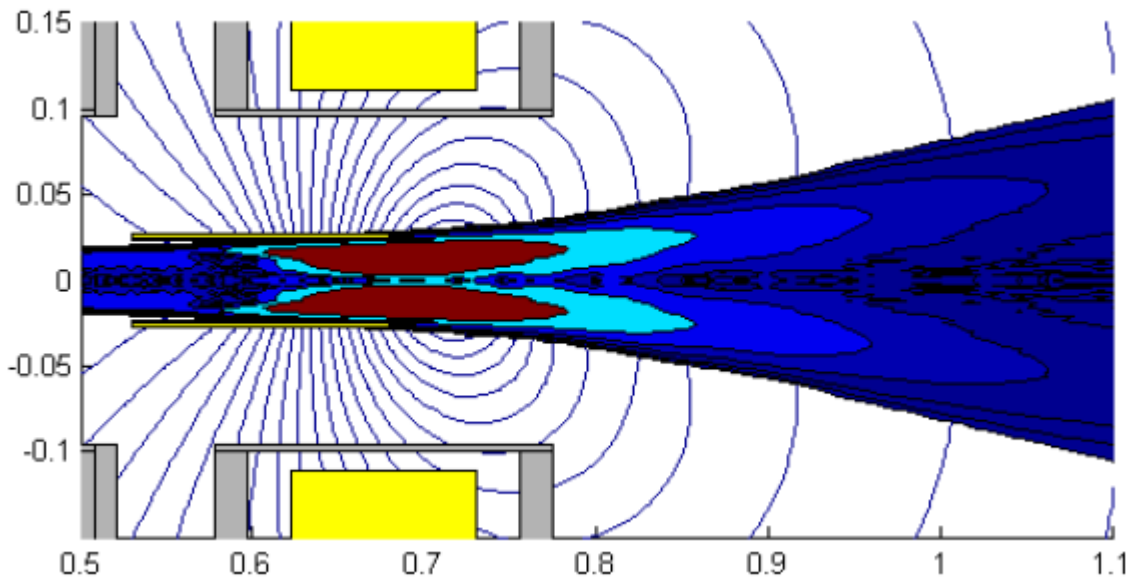


Figure 37 2D contour plots of the diamagnetic current density  $j_{p,\phi}$ , calculated by the particle trajectory code and the magnetic field lines for the corresponding diamagnetic plasma field  $B_p$  Source: Ilin, 2003

Figure 37 demonstrates the plasma diamagnetic current and the magnetic field calculated by equation 20. The diamagnetic effect is essential only for high magnetic field in the area close to the thruster core and becomes negligible further away from it.

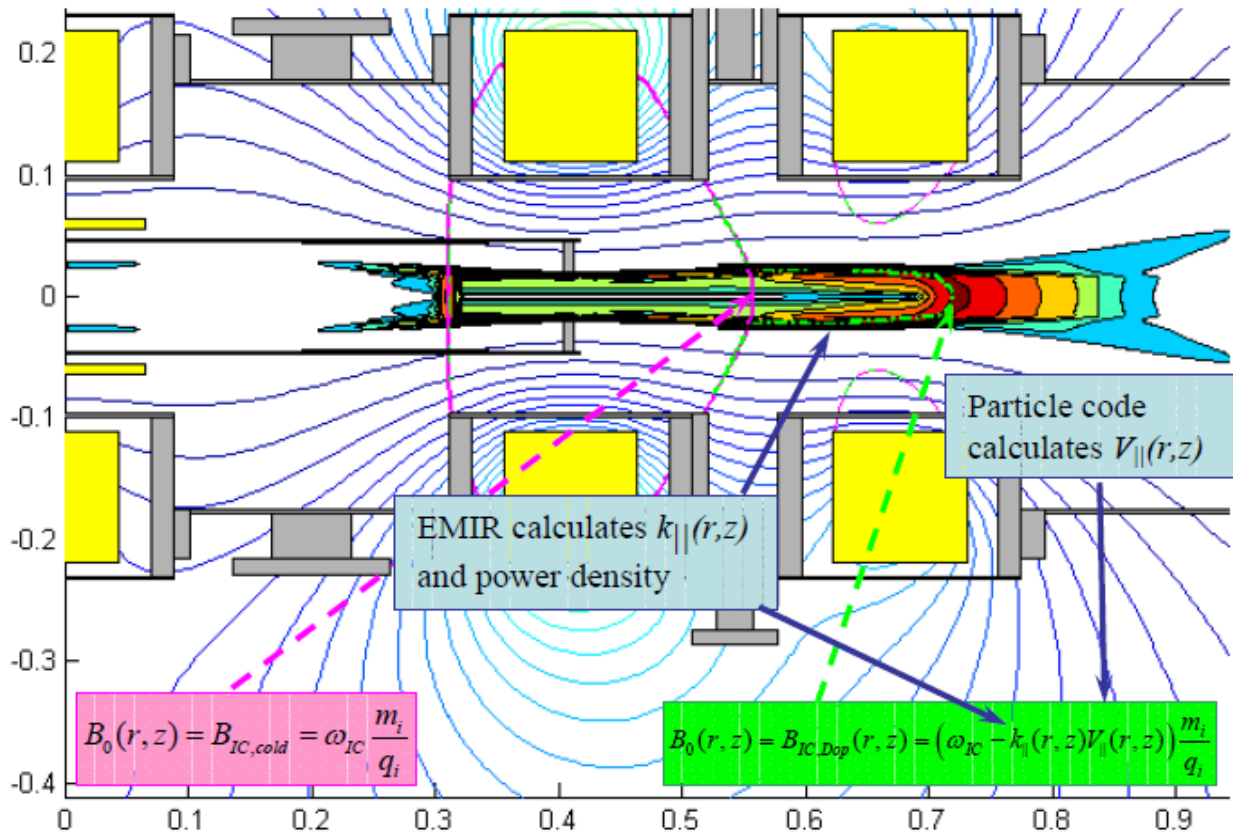


Figure 38 2D plot of the magnetic induction configuration for the VASIMR Source: Ilin, 2003

Figure 38 shows the power density vs. longitudinal coordinate features a peak shifted downstream from the cold plasma ion cyclotron resonance due to the Doppler Effect. Most of the power gets absorbed by the plasma at the Doppler-shifted resonance.

## 5.6 Mission Analysis

The power-limited equations for the interplanetary vehicle will be described here briefly. More detailed descriptions are provided by Irving and Melbourne. The thrust, “ $T$ ,” the power in the thrust beam, “ $p$ ,” the specific mass of the power plant, “ $m_w$ ” and the thrust acceleration, “ $a_T$ ,” for power-limited systems are written,

$$T = \dot{m}_p c \quad (22)$$

$$p = \frac{1}{2} \dot{m}_p c^2 \quad (23)$$

$$a_T = \frac{\dot{m}_p c}{m} \quad (24)$$

$$\alpha = \frac{m_w}{P} \quad (25)$$

$$P = \frac{p}{\varepsilon} \quad (26)$$

Where  $\dot{m}$  is the propellant mass-flow rate, and  $c$  is the exhaust velocity. This quantity is related to the specific impulse “ $I_{sp}$ ” through the familiar relation:  $c = g \cdot I_{sp}$ , where  $g$  is the acceleration of gravity at the Earth’s surface,  $9.8 \text{ m/sec}^2$ . The remaining quantities are the total spacecraft mass, “ $m$ ,” the power plant mass, “ $m_w$ ,” and its power rating, “ $P$ .” Propellant mass-flow rate of  $130 \text{ mg/s}$ , Exhaust velocity of  $50 \text{ km/s}$ , Power plant mass of  $1200 \text{ kg}$ , Total mass of  $34 \text{ Tone}$  and  $\alpha$  Of  $0.6 \text{ kg/W}$  were used to find the rest of the values in above equations which results in:

Thrust beam power of  $162.5 \text{ kW}$  and  $\varepsilon$  of  $0.81$ , whereas the Thrust acceleration was found to be  $0.154 \text{ m/s}$ .

A rocket equation for power-limited propulsion systems can be written from the above equations by solving for “ $(a_T)^2$ ” and then integrating over time as follows: (Diaz, 1995)

$$\frac{1}{m(t)} = \frac{1}{m_0} + \frac{\alpha}{2m_w \varepsilon} \int_{t_0}^t a_T^2 \cdot dt \quad (27)$$

Where “ $m(t)$ ” is the spacecraft mass at time, “ $t$ ,” “ $m_0$ ” is the initial spacecraft mass, and “ $\varepsilon$ ” is the power plant efficiency. The vehicle parameters can be separated from the trajectory parameters and the rocket equation can be rewritten as:

$$\frac{1}{m(t)} = \frac{1}{m_0} + \frac{1}{m_w} \beta(t)^2 \quad (28)$$

$$; \quad \beta(t)^2 = \frac{\alpha}{2\varepsilon} \int_{t_0}^t a_T^2 \cdot dt \quad (29)$$

$$\text{at, } t=t_f \quad [\beta(t_f)]^2 = \frac{\alpha}{\varepsilon} J^2 \quad (30)$$

$$; \quad J^2 = \frac{1}{2} \int_{t_0}^t a_T^2 \cdot dt \quad \text{is the performance index.} \quad (31)$$

The trajectory is optimized independently of the vehicle by minimizing  $J^2$ , which effectively minimizes the amount of propellant required for the mission. (Williams, 2001) This optimized trajectory is then used with the vehicle parameters, which are determined by the mission planner, to calculate the power plant and payload mass fractions. The spacecraft mass at any time, “ $t$ ,” is equal to the sum of the payload mass, “ $m_L$ ,” the power plant mass, “ $m_w$ ,” and the propellant mass, “ $m_p(t)$ .”

$$m(t) = m_L + m_w + m_p(t) \quad (32)$$

The initial propellant mass, “ $m_p(0)$ ,” is assumed to be exactly the amount of propellant necessary to complete the mission, so at the end of the mission,  $m_p(t_f) = 0$ .

## 6.0 Conclusion and Recommendations

### Conclusion

The project work gave an opportunity to study and a chance to work on one of the latest and most efficient rocket engine up to the date which is still in the development stage.

1. The designed rocket geometry shows that proposed rocket is small compared to conventional rockets.
2. The VASIMR rocket with the  $I_{sp}$  of 5000 sec, Force of 5 Newton per engine, coupled power of 200kW and 78% thruster efficiency is capable of taking 34.7 tone weight to Mars in approximately 39 days.
3. Although it is very complicated and challenging to operate in high temperatures, the VASIMR engine would be less expensive and could bring a revolution in space missions. Some performance parameters of the engine performance are calculated based on the available data and equations.
4. Flux density, Ion density, Ion velocity in different magnetic field and temperature are the topics in early stage of research.

### Recommendations

1. Using heavier species like Nitrogen, Ammonia, and water are the possible candidates of propellant as they are denser and can produce dense plasma.
2. Efficiency of ICRF booster stage increases with the increase in plasma density. Plasma density can be increased by additional gas input and increased helicon stage power input.
3. Use higher coupled voltage more than 200kW should be developed with more improved thruster efficiency.
4. Mass flow rate should be increased in order to get more thrust force.

## **References:**

AdAstra rocket company (2010). Vasimr VX-200 meets full power efficiency milestone,

Retrieved on August 18, 2010 from Website: [adastrarocket.com](http://adastrarocket.com)

ADAstra rocket company (2010) Retrieved on: August 31,2010

from: [www.adastrarocket.com/aarc/Technology](http://www.adastrarocket.com/aarc/Technology)

Andrew V. Ilin\*, Franklin R. Chang Díaz†, Jared P. Squire, Plasma Heating Simulation in the

TX 77059. Plasma rocket. (2010,). Retrieved from:<http://aerorocket.com/plasmarocket.html>.

VASIMR System, Advanced Space Propulsion Laboratory, JSC / NASA, Houston, TX

Atkov, O., Burke, J., Dator, J., Hall, T., Kanas, N., Pierre, J., Logsdon, J., Mckay, C., Nelson, I., Peter, N., Petit, P., Riester, M., Russell, C., Rycroft, M., Sponberg, B., Thronson, H., Vivanco, S., Winglee, R., Woodburn, T. (2004). Human Missions to Europa and Titan — Why Not? International Space University. MSS'04.9. 13-19, 29-78.

Baity, F., Barber, G., Carter, M., Goulding, R., Sparks, D., Chang, F., McCaskill, G., Squire, J., (2003) Design of RF systems for the RTD mission VASIMR, Oak Ridge Laboratory, Oak Ridge, TN 37831 ASPL, NASA, Johnson Space Center, Houston, TX 77059

Bering, E., Brukardt, M., Squire, J., (2006) Recent Improvements in Ionization Costs and Ion Cyclotron Heating Efficiency in The VASIMR engine. AIAA-2006-766

Blackwell, D., Chen, F., (1997). 2D imaging of a helicon discharge. Electrical Engineering department, University of California, Los Angeles, California 90095-1594

Cassady, L., Longmeir, B., Olsen, C., Ballenger, M., McCaskill, G., Diaz, F., Glover, T., Ilin, A., Carter, M., (2010). VASIMR Performance Results. AIAA 2010-6772

Chang, F. (2010). The VASIMR. Scientific American, 283(5), page: 90-97

Cipolla, J. (2008). Aerorocket. (January, 2008) Star Travel 3.0 Technical Instructions.

Clark, K., Magner, T., Pappalardo, R., Blanc, M., Greeley, R., Lebreton, J., Jones, C., Sommerer, J., (2009). Jupiter Europa Orbiter Mission Study. National Aeronautics and Space Administration. Task Order #NMO710851. 12-27.

Diaz, F., Hsu, M., Braden, E., Johnson, I., Yang, T., (1995). Rapid Mars Transits With Exhaust Modulated Plasma Propulsion. NASA technical paper 3539

Diaz, F., (2000). The VASIMR. An article from Scientific American. VOL. 283 NO.5

Edgar, A. (2010). Recent improvements in ionization costs and ion cyclotron heating efficiency in the VASIMR engine. Houston, TX: Adastrarocket company

Executive Summary. (2008) Ad Astra rocket company. Retrieved on: March 14, 2010 from: [adastrarocket.com](http://adastrarocket.com)

Franklin R. Chang Díaz, Ellen Braden, and Ivan Johnson Lyndon B. (2010) Rapid Mars Transits With Exhaust- Modulated Plasma Propulsion. NASA Technical Paper 3539, Johnson Space Center Houston, Texas

Glover, T., Diaz, F., Squire, J., Jacobson, V., Chavers, D., Carter, M., (2000) Principal VASIMR Results and Present Objectives. NASA ASPL, TX 77059

Google (2010), Retrieved on May, 2010 from: [google.com/images/mars](http://google.com/images/mars)

Ilin, A., Diaz, F., Squire, J., (2005). Plasma Heating Simulation in the VASIM system. ASPL, TX. AIAA-2005-0949

Leonard D. Cassady, Benjamin W. Longmiery, Chris S. Olseny, Maxwell G. Ballengery, Greg E. McCaskillz, Andrew V. Ilinx, Mark D. Carter, Tim W. Gloverk, Jared P. Squire D., Franklin R. Chang D. VASIMRR Performance Results. Ad Astra Rocket Company, 141 W. Bay Area Blvd, Houston, TX 77598, USA

Mars exploration. (2010), Retrieved from: <http://nssdc.gsfc.nasa.gov/planetary/mars>

Marshall, A., Hendrickson, C., Jackson, G., (1998) Fourier Transform Ion Cyclotron Resonance Mass Spectrometry: A Premier. Center for Interdisciplinary Magnetic Resonance, National High Magnetic, Florida State University, Tallahassee, FL 32310

Maxfield, B., (1968). Helicon Waves in Solids, American Journal of Physics.

Vol.37 #3.(Retrieved Oct 16, 1968) Laboratory of Atomic and Solid-State Physics, Cornell University, Ithaca, NY 14850

NASA- National Aeronautics and Space Administration, JPL- Jet Propulsion Lab.

Retrieved March 18, 2010, from the NASA/JPL

Website: <http://mars.jpl.nasa.gov/odyssey/mission/science/>

NASA- National Aeronautics and Space Administration.

Retrieved March 24, 2010, from the NASA

Website: [http://www.nasa.gov/worldbook/Europa\\_worldbook.html](http://www.nasa.gov/worldbook/Europa_worldbook.html)

Squire, J. Diaz, F., Carter, M., Glover, T.,(2007). High Power VASIMR Experiments using Deuterium, Neon, and Argon. IEPC-2007-181

VASIMR Press release 011009. (2009) Retrieved on August 28, 2010 from

Website: [asastrarocket.com](http://asastrarocket.com)

VASIMR Press release 241008. (2009) Retrieved on September 13, 2010 from

Website: [asastrarocket.com](http://asastrarocket.com)

Williams, C., Dudzinski, A., Borowski, S., Juhasz, A., (2005). Realizing “2001: A Space Odyssey”: piloted spherical torus nuclear fusion propulsion. Glenn research center, Cleveland, Ohio. NASA/TM- 2005-213559

Zelenyi, L., Martynov, M., Korablev, O., Fedorova, A., Sukhanov, A., Podzolko, M., Simonov, A., Lomakin, I., Popov, G., Akim, E., and Europa Lander Team (2010) Galileo’s Medician

Moons: Their Impact on 400 Years of Discovery. IKI, NPOL, Skobeltsyn Institute of Nuclear Physics, MSU, Keldysh Institute Applied Mathematics.44-179.